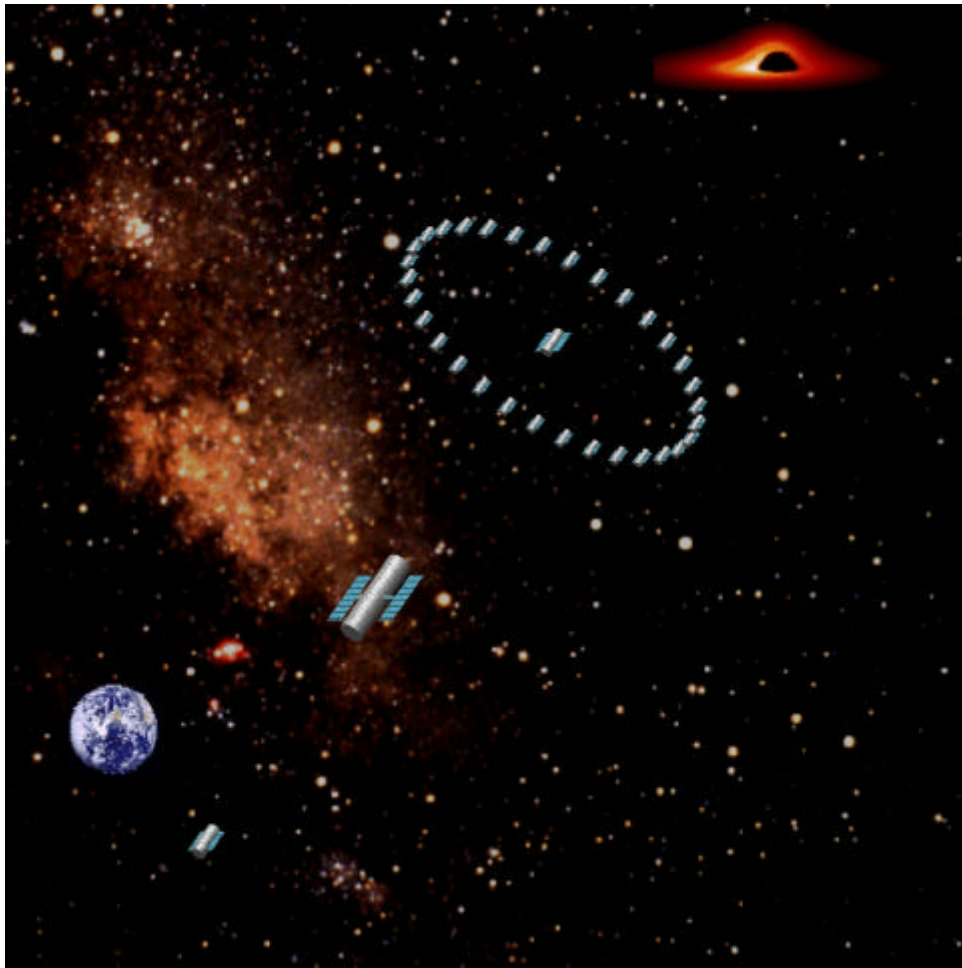# Final Report to the
NASA Institute for Advanced Concepts
April, 2002

Phase II Study

X-ray Interferometry

Ultimate Astronomical Imaging

Webster Cash
University of Colorado

Boulder, CO 80309
303-492-4056
cash@casa.colorado.edu

Personnel

Principal Investigator Webster Cash, University of Colorado

Co-Investigators: Dennis Gallagher, Ball Aerospace
        Steven Kahn, Columbia University
        Mark Schattenburg, MIT
        David Windt, Columbia University
        Michael Lieber, Ball Aerospace
        Ann Shipley, University of Colorado

Table of Contents

Summary

At the time we wrote our proposal to NIAC, conventional wisdom had x-ray interferometry as a practical impossibility. With NIAC's help, the conventional wisdom has shifted. X-ray interferometry is possible, just very expensive. And now we are working on bringing the price down.

We now know how to build an affordable x-ray interferometer that, using existing technology, can exceed the resolution of the Hubble by a factor of a million and capture an image of black hole.

We have demonstrated a laboratory model, defined a mission architecture, carried the word to the community, and made Maxim (the Micro-Arcsecond X-ray Interferometry Mission) part of the NASA planning.

I. Goals

A. Science

The x-ray band, contrary to popular opinion, is actually a natural place to perform interferometry and observe targets at the highest angular resolution. There are two major advantages that x-rays hold over imaging at longer wavelengths.

First, because the wavelengths are a thousand times shorter than the visible, the baselines required are similarly short. For example, in order to achieve resolution of 100 micro-arcseconds at 1keV, we need an interferometer with a baseline of about 1.4 meters, achievable in a single spacecraft. For comparison, to achieve the same resolution in the radio at 6cm wavelength would require 120,000 kilometers. At 5000Å, the required baseline is already a kilometer.

The second advantage of x-rays is the intrinsic brightness of many of the sources. X-ray sources are considered faint, but that is largely because of the small region from which the x-rays emanate. For example, a mass transfer binary can emit 10,000 solar luminosities of x-rays from a region that is only .0001 solar areas in extent. It is emitting 100 million times more energy per unit surface area. Even allowing for the high energy content per photon, the x-ray source emits 100,000 times more photons per unit area. This means that when we look at tiny objects, the telescope collecting area required is much lower in the x-ray.

The major disadvantage of the x-ray so far has been our failure to build diffraction limited optics that can be used to construct a sensitive x-ray interferometer. But recent advances have demonstrated in the laboratory that such optics are feasible and have shown us a technical roadmap that leads to long baseline x-ray interferometry observatories.

The range of science addressable at resolutions of 0.1milli-arcseconds and below is broad, and just a few of the goals are presented in Table 1.

Table 1: Science Goals

| Target Class	Goal
Resolve the coronae of nearby stars	Are other coronal structures like the solar corona?
Resolve the winds of OB stars	What kind of shocks drive the x-ray emission?
Resolve pre-main sequence stars	How does coronal activity interact with disk?
Image center of Milky Way	Detect and resolve accretion disk
Detailed images of LMC, SMC, M31	Supernova morphology and star formation in other settings
Image jets, outflows and BLR from AGN	Follow jet structure, search for scattered emission from BLR
Detailed view of starbursts	Resolve supernovae and outflows
Map center of cooling flows in clusters	Resolve star formation regions
Image Event Horizon of Black Hole	Study Material in Extreme Gravitational Limit
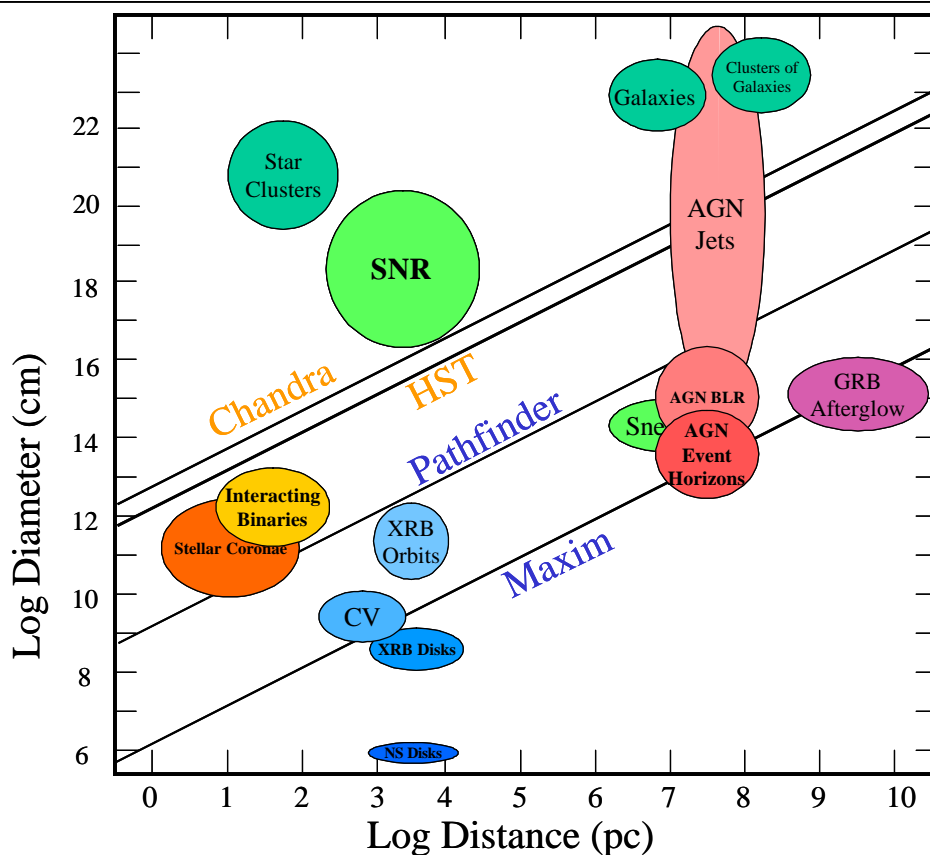
Figure 1 A classic "bubble diagram" for astronomy. Along one axis we plot the distance to a typical example of a class of target. Along the other axis is the characteristic size. Then resolution is found as a straight line on the diagram. HST, the highest resolution observatory in orbit is shown, as is Chandra, the best x-ray observatory.

What the diagram shows is that **ALL** observatories to date take images of interstellar phenomena only. We can image galaxies, star clusters, and interstellar gas bubbles, but the individual objects which either drive or make up the large structure are unresolved. Astronomy will enjoy a revolution when telescopes finally resolve stars and other compact objects.

B. Requirements

The basic requirements for an x-ray interferometry mission are shown in Table 2. In order to achieve resolution of 100 micro-arcseconds at 1keV, we need an interferometer with a baseline of about 1.4 meters, obtainable in a single spacecraft. For comparison, to gain the same resolution in the radio at 6cm wavelength would require 120,000 kilometers.

Table 2: Performance Requirements

Angular Resolution	100µas	100nas
Baseline	1.4 meters	300meters
Collecting Area	100cm^2	3000cm^2
Field of View	10 mas	10µas
Bandpass	0.5-2keV + 6keV	0.5-6keV
Pointing	30µas	30nas
Spectral Resolution (E/δE)	20	1000
Size	2 craft	Dozens of craft

The science requires that we be able to observe at 1keV, since many of the most interesting targets are obscured below 0.5keV by absorption in the interstellar medium. Adding some capability at 6keV through the use of multilayers would be very exciting, giving the mission access to the astrophysically-important Fe K line. The collecting area should be in the vicinity of 100cm^2. We know from previous missions like *Einstein* that 100cm^2 supports excellent work on a large variety of objects. However, missions with just 10cm^2 of collecting area have studied a limited range of bright targets.
We do not expect or need to move to new targets hourly. A new target every few days would allow the mission to return a spectacular set of about one hundred unique images per year. Thus modest collecting area and leisurely target acquisition are acceptable.
The stability requirements on the spacecraft are quite challenging. There is little hope of suppressing all the extraneous mechanical influences of low Earth orbit, so it appears that either a high orbit or a drift-away orbit will be required. These high orbits naturally allow lengthy observations of targets, which is valuable for high quality image reconstruction.

II. Maxim

Throughout the effort we have been working closely with the Goddard Space Flight Center and with the astronomy community's planning committees, attempting to spread the word of x-ray interferometry. These efforts have helped crystallize MAXIM, the Micro-Arcsecond X-ray Imaging Mission, within the planning at NASA. MAXIM is now

a "Vision Mission" for the future. Maxim Pathfinder, a stepping stone at 100 µas is a mid-term mission. Further information is available on their website at http://maxim.gsfc.nasa.gov.

Nasa Programmatics

As part of its mission to Explore the Universe, NASA has always maintained an aggressive program in space astronomy. But, there are many worthy projects competing for support. We have to prove that X-ray interferometry will fit naturally into this program and that it should be given priority. From a programmatic perspective x-ray interferometry is a good fit. Like all x-ray astronomy, it can only be done from space. However, it provides some challenges to NASA's engineering expertise, including:

- Precision formation flying of multiple spacecraft
- Interferometric pointing control of spacecraft
- Active metrology for high internal spacecraft stability
- Stable drift-away orbital environments
- High precision target acquisition

Luckily, our requirements do not stand alone. All of the above challenges are also being addressed by other missions in NASA's plans. Chief among these are ST-3, LISA, and SIM.

Maxim now appears in the advance planning for the Structure and Evolution of the Universe Space Science theme at NASA. A full capability Maxim, with resolution better than one micro-arcsecond and ability to image event horizons in AGN's is described as a "Vision Mission" for the time period beyond 2015. A more modest mission, called Maxim Pathfinder is planned for a new start as early as 2008.

The Maxim Pathfinder Mission is expected to operate in the 0.5 to 1.5keV band and collect images of x-ray sources with resolution of 100 micro-arcseconds or better. With such a huge leap in capability (representing a thousand-fold improvement over HST) there exist many technical problems to be solved.

III. Architecture & Development Pathway

A. Components of the Architecture

The architecture of an x-ray interferometer can be broken into components that all must play together to make the system successful. These include:

- Grazing Incidence
- Optical Design
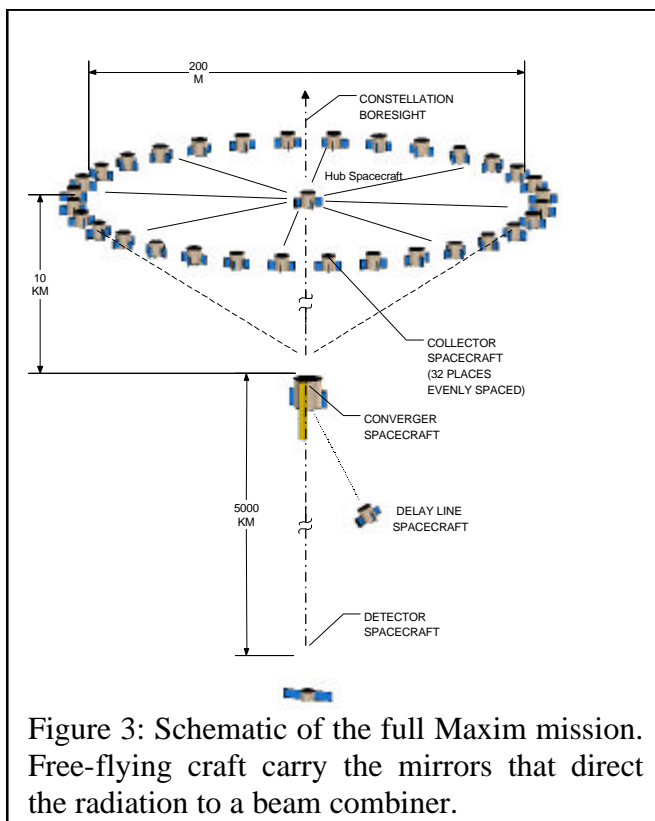- Phase Closure
- Formation Flying

- Mechanical Stability
- Pointing
- Target Acquisition

We have addressed each of these areas during the study and concluded that some are straightforward, and some are more difficult, but all can be handled.

B. The "X" Configuration

Technical Challenges

Supporting the obviously ambitious requirements of Maxim involve solving certain basic challenges. Figure 3 is a schematic of the mission architecture.

Figure 3: Schematic of the full Maxim mission. Free-flying craft carry the mirrors that direct the radiation to a beam combiner.

Formation Flying: To minimize disturbances, the constellation of spacecraft operates in a heliocentric driftaway orbit with a semimajor axis of 1 Au and an ecliptic inclination of zero. To minimize thermal stresses on the S/C, the constellation boresight is always oriented at right angles to the sunline, although it is free to rotate 360 degrees around it.

In operation, the Converger, by far the most massive of the S/C operates in the orbit plane at all times to minimize the constellation's propellant consumption. Depending on the orientation of the constellation boresight about the sunline, the collector S/C position will be in a range from 0 to 10 km from the ecliptic plane. The lightest S/C, the detector, will operate in a range of from 0 to 5000 km from the plane.

To keep the S/C in their correct positions to this level of accuracy for all possible constellation boresight orientations, they must be continuously stationkept against forces exerted by solar radiation pressure and solar gravity.

Aspect Control: A number of alternative, higher specific impulse propulsion approaches exist, among them ion, magneto plasma dynamic, and stationary plasma thrusters. Each potentially offers a factor of four or better reduction in propellant consumption, at the price of an equivalent increase in power draw. Our trade study will define which of these

options provides the best combination of cost and performance for the operational MAXIM constellation.

Mirrors, Mounts, Alignment And Thermal: The interferometer's active area requirement and proposed instrument configuration drive the mirror geometry to a long narrow shape. This represents a challenging mirror shape to mount even with relatively loose surface figure requirements. Current tolerance studies indicate each mirror's surface accuracy will be required to meet $\lambda/100$ rms surface figure with less than 5Å surface roughness. Such an accurate surface figure requirement makes many subtle errors significant in estimating the total wavefront error. An acceptable mounted mirror's $\lambda/100$ surface must include errors due to alignment, thermal gradient, jitter, stability, assembly, manufacturing, test, 1g release, temperature change, temperature gradient, adhesive cure strain, bolt preload, and even the reflective coating thickness variation. Investigating a smaller mirror mount with similar requirements has given us the ability to quantify the errors and environmental effects most likely to become drivers that will require technology development. This approach allows us to break down the problem into smaller parts to identify areas that require technological advancement uncoupled from the known challenge involved with the mirror's size and shape. Additionally, we have completed the analysis for a smaller system that can be built and tested in a scaled down model of the interferometer. Such tests will be imperative to identifying real-time alignment, thermal, imaging, vibration/jitter, and other unknown subtleties requiring early attention that may not be apparent through analyses.

The analysis of a smaller mirror mount with similar requirements and analytical results indicate a $\lambda/400$ rms ($\lambda/100$ PV) surface figure is reasonably attainable for a 50mm square mirror made of fused silica. Wavefront error analysis based on those analytical results suggest the most challenging factors include: thermal gradient, and piston and tilt error associated with a bulk temperature increase (optical surface distortion is reasonable). The estimated allowable thermal gradient between the front and back of a mirror may be less than 0.01°C. The piston and tilt error of the mirror associated with a change in the stabilized temperature will probably drive the allowable time length of an observation. The mirror positions will need to be corrected between observations to maintain equal pathlengths. The mirror substrate thermal gradient will be difficult to maintain because heat emitted by motors used to manipulate the mirror position will make temperature difficult to stabilize. Materials with improved thermal properties could make this problem more easily contained in the future. Motors capable of high-resolution, stability, and position knowledge that emit very little heat would also help.

The long narrow mirrors will have the same thermal challenges at a much greater magnitude. A challenging parameter for a small mirror certainly indicates an imperative need for technological advancement to support similar requirements in a much larger mirror. Other factors we expect to be difficult are gravity release, stability due to jitter (a function of the mirror's fundamental frequency and mode shape), and the ability to test the mounted mirror's surface figure. The mirror size and high surface accuracy require a test apparatus beyond standard laser interferogram capability.

Active alignment of the optics on-orbit will be critical to maintaining such ambitious resolving power. Our studies using a single channel instrument consisting of four small

mirrors have uncovered alignment issues that will apply to each channel of the instrument. Every mirror in the interferometer will require on-orbit motion in three degrees of freedom (tip, tilt, and piston). Current tolerance studies indicate optic alignment in the remaining three degrees of freedom may withstand launch. Attaining equal pathlengths in each channel will require tilt and piston control of each mirror at an estimated 10 nanometer resolution and knowledge. Equalizing pathlengths in numerous channels simultaneously while providing positional stability over the length of an observation may certainly be considered challenging. Developing continuous on-orbit automated sensing and correction to maintain equal pathlengths in each channel of the interferometer simultaneously could eliminate or greatly reduce these effects. The advent of this capability at the nanometer level would provide incredible imaging capability.

Thermal stability requirements will be a function of the length of time during which each channel's pathlengths may not be optimized. This time constraint may lend itself to the time length of an observation. Continuous automated sensing and pathlength correction could loosen some of these thermal requirements making longer observation sessions a reality. Investigating this avenue as part of the system analysis would be beneficial. A clever mirror mount may minimize wavefront error due to thermal changes, but still cause tip, tilt and piston motions that will far exceed allowable tolerances. Once again this thermal issue may be mitigated with the advent of automated alignment corrections. The thermal challenges are significant, but appear to be integrally tied with mirror, mount, and alignment solutions.

Calibration: It may not be possible to fully calibrate the instrument on the ground. The longest vacuum tank we have available is the XRCF at MSFC, which is 500m. Resolution of one micro-arcsecond at that distance represents a size scale of 2.5nm. We cannot currently even create mask features this fine. We may have to check components, and then perform an in-orbit checkout.

For the development and testing phase of the mission a critical task is to fabricate high-quality target apertures designed to test the diffraction-limited performance of the optical system. The idea is to use microscope optics to image backlit apertures onto the detector. Target apertures of various shapes are useful, such as holes, slits, cross and wagon wheel patterns, and gratings. In order to fully test the optical system, apertures need to be cut into thin, x-ray opaque foils, and need to have sub-micron feature sizes with sharp edges and corners. Specialized laboratory facilities are required to fabricate targets of this quality. MIT is actively engaged in developing these test masks as part of this NIAC study.

StationKeeping: The stationkeeping approach described using existing technology can provide at least a 20 year life for all requirements except along-boresight control for the Detector S/C. The baseline 20 year life could be doubled by simply adding a second set of thrusters to each axis. Accordingly, these requirements are not considered limiting.

Limits are completely dominated by Detector S/C along-boresight control. For equivalent lifetime, total impulse requirements are a linear function of the distance along the boresight; a 10,000 km distance would require twice the total impulse or reduction of the mission lifetime to 5 years. Removing these limits could be accomplished by adding

more PPT's, or by using a higher specific impulse propulsion approach such as ion or magneto-plasma-dynamic thrusters. In any case, an absolute limit imposed by propellant load would probably be reached at between 50,000 and 100,000 km separation.

Aspect Information: We expect to obtain aspect information by using a Michelson flat at the hub spacecraft to redirect the signal from a stellar object into an interferometer on the converger craft. As the array flies apart, the baseline of this interferometer grows along with the baseline of the x-ray interferometer. Two effects can limit the effectiveness of this aspect interferometer.

First is the diffraction from the Michelson flat. A ten meter optic will cause visible light to diffract one part in $2x10^7$. If the beam is to diffract to less than 100m across, resulting in a factor of 100 loss in signal, then the baseline of the aspect interferometer can be as high as 2 million kilometers. This indicates an x-ray interferometer with a baseline of 200,000km and resolution of 10^{-17} radians.

The other effect is the size of the star being used to provide the reference wavefront. We rapidly start to run out of thermal reference information in the visible portion of the spectrum. We can use main sequence stars at a distance as great as 10,000pc, which have an angular extent of around 10^{-11} radians, which will be resolved across a baseline of 100km. We could use white dwarf stars, but, while they are smaller, they are also dimmer, and we cannot see them a great distances. Similarly, the visible emission of AGN's is too extended. This problem is a direct result of the relative faintness of visible emission from objects. The only hope to solve this problem in the visible is to observe non-thermal objects such as pulsars. The Crab pulsar is detectable in the visible, yet is only a few kilometers across, so might give us the needed information. At a diameter of 10km at 2kpc, it has an angular extent of 10^{-16} radians, a reasonable match to the x-ray resolution.
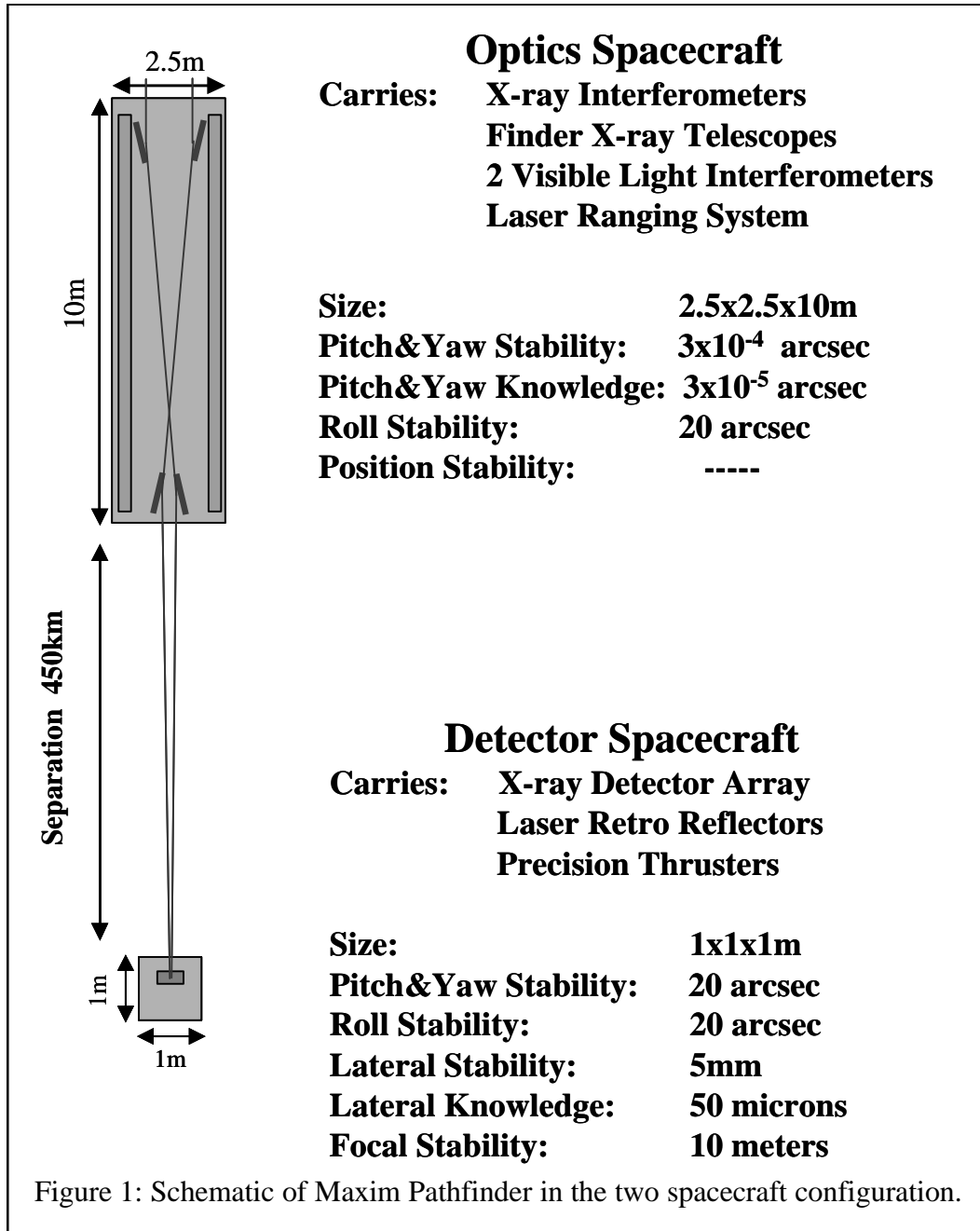
Of course, we can solve the problem by getting our aspect information from an x-ray interferometer. We are looking at this as an option.

C. The Pathfinder Mission Concept

Pathfinder consists of an array of grazing incidence mirrors on a stabilized spacecraft, creating x-ray interference fringes on the detector, which is located on a second spacecraft 450km away.
The Optics: Mirrors that preserve the x-ray wavefront are very difficult to polish and figure, even at grazing incidence. While it is *possible* to build Wolter-type x-ray telescopes that are diffraction limited, these greatly complicate the fabrication of the observatory and depress the collecting area. For this reason we have chosen to use the flat mirror concept. The interferometer will consist of two rings of flat mirrors. Each ring will contain 32 flat mirrors, each fine adjustable to achieve zero null on axis. The interferometer will have about 100cm^2 of effective collecting area, similar to that of Einstein and ROSAT.

Target Acquisition: Most of the science targets will boast celestial coordinates accurate to only slightly better than one arcsecond, but Pathfinder must have a way to allow the observer to center on the target of interest. As such, Pathfinder will have two x-ray optical systems, a Wolter telescope and an interferometer. The Wolter telescope will have approximately five arcseconds resolution while the interferometer will have a 1.4 meter

Optics Spacecraft

Carries: **X-ray Interferometers**
Finder X-ray Telescopes
2 Visible Light Interferometers
Laser Ranging System

Size:	**2.5x2.5x10m**
Pitch&Yaw Stability:	**$3x10^{-4}$ arcsec**
Pitch&Yaw Knowledge:	**$3x10^{-5}$ arcsec**
Roll Stability:	**20 arcsec**
Position Stability:	**-----**

2.5m

10m

Separation 450km

Detector Spacecraft

Carries: **X-ray Detector Array**
Laser Retro Reflectors
Precision Thrusters

Size:	**1x1x1m**
Pitch&Yaw Stability:	**20 arcsec**
Roll Stability:	**20 arcsec**
Lateral Stability:	**5mm**
Lateral Knowledge:	**50 microns**
Focal Stability:	**10 meters**

1m

1m

Figure 1: Schematic of Maxim Pathfinder in the two spacecraft configuration.

baseline and produce the full 100 micro-arcsecond resolution. The detector spacecraft will have a 30x30cm array of CCDs. The size of the 3cm beam cast by the mirrors at a distance of 450km is only about 15 milli-arcseconds. The array of detectors increases this coverage to about 150 milli-arcseconds. If the Wolter telescope has resolution of about

five arcseconds, then it should be possible to centroid the target to about 0.15 arcseconds. The first image with the interferometer can then be used to center exactly on the target.

Optics Spacecraft: The spacecraft that carries the interferometers should be about 2.5 meters in diameter and ten meters long. In most respects, such as power and mass, it will be conventional. In the area of pointing stability it must be exceptional. We need to hold the pointing stable to about 300 micro-arcseconds and provide pointing information down to about 30 micro-arcseconds. Drifts greater than 30 micro-arcseconds must not occur during the readout time of the CCD. The pointing information will be generated by two visible light interferometers that will view stars that lie in the heavens approximately perpendicular to the target line of sight and to each other.

Detector: We have investigated an imaging quantum calorimeter for the detector. It needs to be about 30mm square with 200 micron or smaller pixels. Energy resolution of 10eV at 1keV would nicely support the science. However, CCD detectors, with resolution of 50eV would be less expensive and could support the mission. The optics have a very wide field of view, so an array of these 3cm CCD's will be used to increase the field for centroiding on poorly known target positions.

Formation Flying: The detector spacecraft needs to hold its position in space relative to the main spacecraft, to about a tenth of a fringe spacing. This can be accomplished using a laser ranging system between spacecraft and microthrusters to offset drifts. This capability is comparable to that needed in the LISA mission, but is in some ways easier as they need to measure acceleration while we care only about position.

Table 3: Interferometer Characteristics

Primary Ring Diameter	140cm
Secondary Ring Diameter	30cm
Distance: Primary to Secondary	1000cm
Distance: Secondary to Detector	450km
Mirror Size	3x90cm
Graze Angle	2 degrees
Number of Primary Mirrors	32
Number of Secondary Mirrors	32
Mirror Quality @ 6328Å	λ/400
Mirror Coating	Ir + Multilayer
Resolution @ 0.25keV	360 μas
Resolution @ 1keV	90 μas
Resolution @ 6keV	15 μas
Fringe Width @ 1keV	2mm
Fringe Width @ 6keV	0.3mm
Field of View	10 mas
Bandpass	0.1-2keV+6keV

Orbit: Because the two spacecraft need to be stable relative to each other and to the celestial sphere, we must move the mission away from the turbulence of low Earth orbit. We expect that either a flyaway orbit or a Lunar Lagrangian point would be appropriate.

1. Layout

To avoid the potential difficulties of building diffraction limited Wolter x-ray optics, we have baselined the flat mirror interferometer in the "x" configuration as demonstrated in the laboratory. Table 3 summarizes the characteristics of the interferometer design, while Figure 5 shows the layout of such a system schematically in two dimensions. Figure 6 shows a 3D perspective.

This reduces the optics problem to its absolute minimum. Flats are the easiest mirrors to fabricate and to align. The problem is that to achieve adequate fringe magnification the beams must cross at a very low angle. To magnify 1nm waves to 100 micron fringes requires a cross angle of about 2 arcseconds, which implies that L will be large.
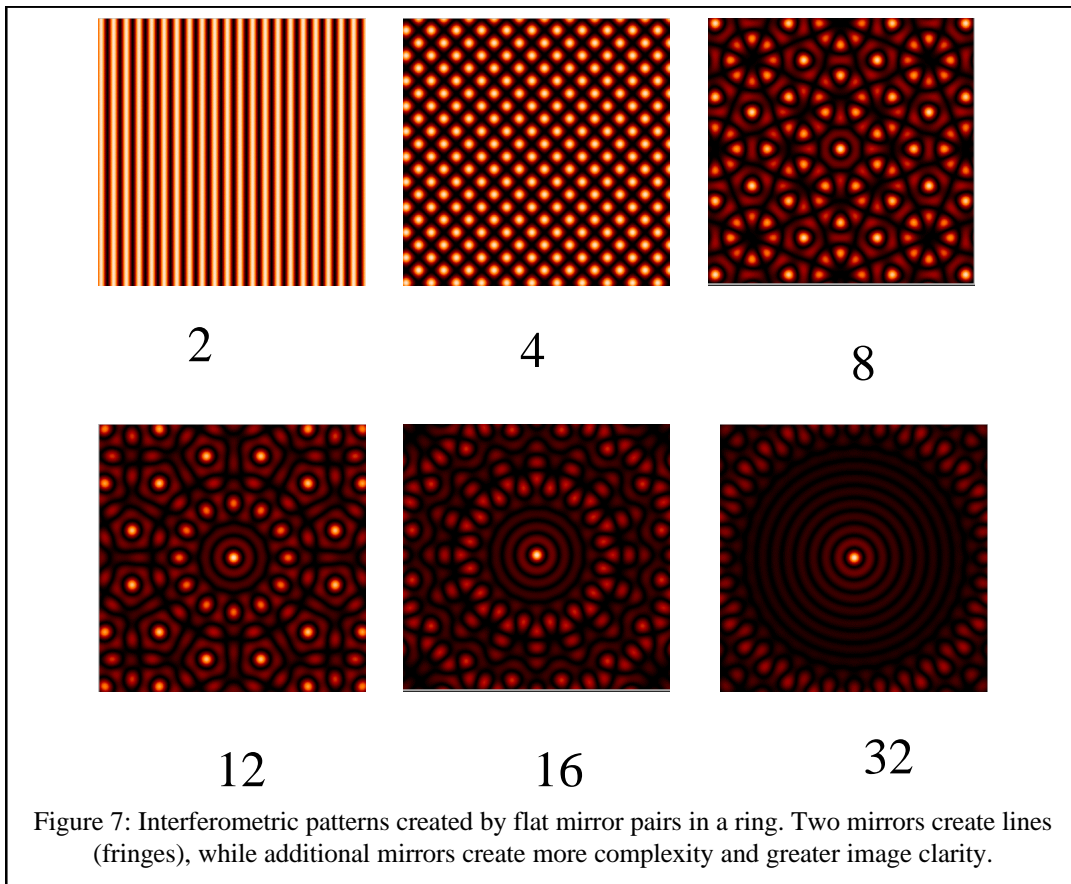

Figure 5: The basic arrangement of the interferometer involves four flat mirrors in an "x" shaped configuration.
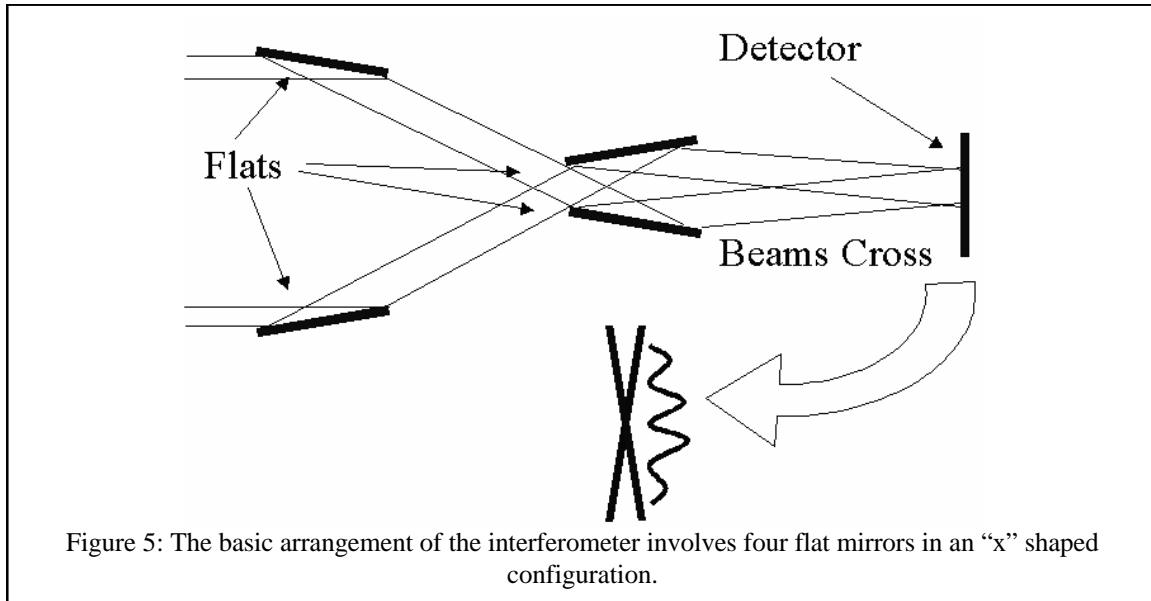
The size of L is in turn driven by the size of d, the spacing between the flats in the beam converger. Our design requirement of $100cm^2$ enters here. We will need 32 flat mirrors in a ring to achieve a nice field of view, so each mirror channel should have about $3cm^2$ of effective area. Allowing for losses due to the two reflections and the detector, we find the aperture should be 3cm square. Fitting 32 such mirrors in a ring requires a 30cm diameter, which we use as the baseline separation in the beam converger.

The effect of bringing 32 flats in a ring into phase coherence is dramatic as shown in Figure 7. The figure is a simulation of the pattern resulting from a monochromatic point source. With two mirrors the detector records the expected sine wave. With four mirrors we find a checkerboard. As the number of mirrors rises, the pattern first becomes complex, and then starts to clear out the region around the central point of constructive interference. We are, effectively, building a diffraction limited telescope out of flat subapertures. As the pointing changes, the bright spot moves around the field of view just as in a telescope. For the 32 mirror case, an excellent image 64x64 pixels in extent is achieved without inversion of fringes. For wider fields of view, there is a substantial

Figure 6: Rendering of the two rings of mirrors shown with 8 mirrors per ring.
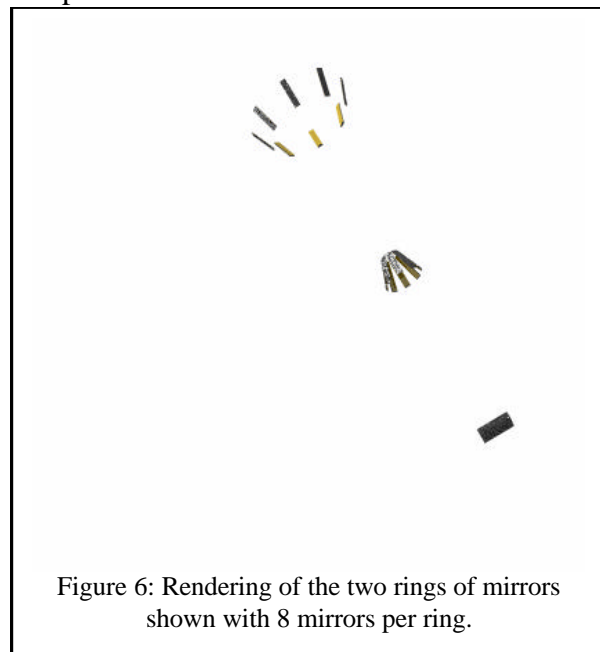
power to be found in the surrounding rings, that must be removed through image processing.

Thus, an interferometer consists of two rings of flat mirrors. In Figure 3 we show a 3-D rendering of the arrays. We show only 8 mirrors per ring for clarity, when the interferometer will have 32 per ring. Each mirror will be mounted on precision actuators that will allow in-flight alignment. The mirrors themselves will be 3cm wide and 90cm long. They can be as thick as desired because there is no nesting envisioned. The total

Figure 7: Interferometric patterns created by flat mirror pairs in a ring. Two mirrors create lines (fringes), while additional mirrors create more complexity and greater image clarity.

amount of glass in each interferometer is about the equivalent of a 1m square mirror.

The primary ring of the interferometer will consist of 32 mirrors with actuators in a ring 1.4 meters in diameter. The resolution of such a ring is given by $\lambda/2D$, where D is the diameter of the ring. This supports resolution of 70μas at 1nm, and 100μas at 0.9keV. At 6keV, using the multilayer reflection, the resolution reaches 14μas.

Note that the resolution is given as $\lambda/2D$, not the usual λ/D. The usual formula is appropriate for a filled aperture telescope, where, when the outer edges of the mirror are 180 degrees out of phase, most of the center is still in phase. Also, consider that in an interferometer, an angle change of λ/D will cause a the a full fringe shift, but we can resolve two stars when they are half a fringe out of phase, indicating the resolution is $\lambda/2D$. Our use of a single ring creates large diffraction rings, but it also doubles the resolution.

2. Mirror Requirements

An x-ray interferometer is a sensitive device. The lengths of the paths that the x-rays travel are sensitive to errors in position and angle in the mirrors. They have to be held to a fraction of an x-ray wavelength, which means 100 picometers. This would be extremely challenging except that we are once again rescued by the geometry of grazing incidence. In the direction of the mirror normal we find that the position tolerance is relaxed by a factor of $1/\sin\theta$ relative to a normal incidence reflection. For 1nm radiation, we typically use a 2 degree graze angle, which, when inserted into the formula implies that the mirror must be held to about 1.5nm relative to the mirror on the other side of the interferometer if the fringe is to be held to one tenth of a wavelength.

The tightest tolerance is for an angular deviation in the in-plane direction. The figure proves that each mirror should be held to one tenth of its own diffraction limit. This makes sense, as there is no optical information below the diffraction limit except at the fraction of a fringe level. For Pathfinder we find that each mirror must be aligned and held to about one milli-arcsecond if it is to hold the tenth fringe requirement.

This is an area that needs substantial development before flight. The tolerances are stringent and at the state of the art. We need to develop both the mirrors and their holders for flight.

D. Pathway

Figure 8 is the development pathway as presented in our Phase II proposal. All of the components of demonstrating the architecture that are shown as boxes have now been addressed. Much of the information is contained within this report. Except for mission cost and schedule, which are beyond the scope of this general study, each item has been studied and solutions to the problems found. In short, x-ray interferometry has been shown to be viable. The next step is to move to full mission design.

Development Pathway
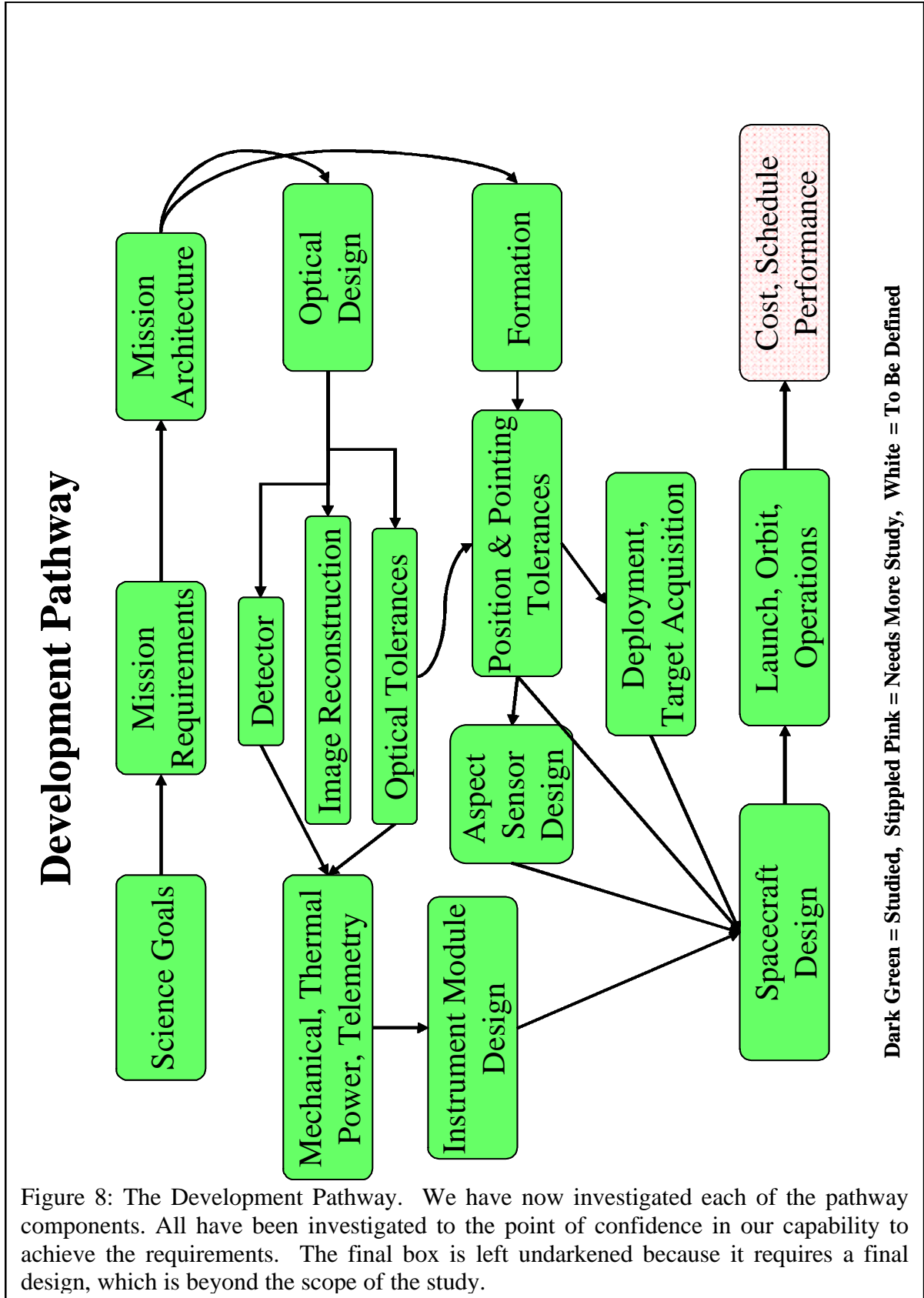
Figure 8: The Development Pathway. We have now investigated each of the pathway components. All have been investigated to the point of confidence in our capability to achieve the requirements. The final box is left undarkened because it requires a final design, which is beyond the scope of the study.

Dark Green = Studied, Stippled Pink = Needs More Study, White = To Be Defined

IV. CU Results

A. Public Results

If x-ray interferometry is to become a reality it needs to enter the consciousness of the astronomy community and of NASA. If there is sufficient support then the missions can enter the long term NASA planning and eventually achieve launch. Through this NIAC support we actively promoted the concept to NASA and the worldwide astronomy community. The audience has been highly receptive. We are making the realities of x-ray interferometry known through the "3 p's" presentation, publicity and publication. Below are some listings of materials that have gone out in support of this effort.

Presentations
- NIAC Annual Meeting Goddard Space Flight Center June 2000
- General Assembly of the International Astronomical Union Manchester England, August 2000
- X-ray 2000 Symposium, Mondello, Italy September 2000
- High Energy Astrophysics Division in Honolulu, November 2000.
- Chancellors Lecture at CU Boulder, December 2000.
- Material presented as part of speech by Mr Goldin, January 2001
- NIST, February 2001
- New Century of X-ray Astronomy, Yokohama, March 2001
- U of Colorado, March 2001
- NIAC Annual Meeting, Mountain View, CA June 2001
- Colloquium, University of Padua, May 2001
- Colloquium, University of Milan, May 2001
- Colloquium, University of Wyoming, July 2001
- Structure and Evolution of the Universe Committee, Presentation on Maxim, December 2001

Publications:
- Shipley, A., Cash, W., Joy, M., "Grazing Incidence Optics for X-ray Interferometry", *Proc. Soc. Photo-Opt. Instr. Eng.*, **4012**, 456-466, 2000.
- Joy, M., Shipley, A., Cash, W., Carter J., Zissa, D., Cuntz, M., "Experimental Results from a Grazing Incidence X-ray Interferometer" *Proc. Soc. Photo-Opt. Instr. Eng.*, **4012**, 270-277, 2000.
- Cash, W., White N., Joy, M., "The Maxim Pathfinder Mission: X-ray Imaging at 100 Micro-Arcseconds", *Proc. Soc. Photo-Opt. Instr. Eng.*, **4012**, 258-269, 2000.
- Windt, D., Cash, W., and Kahn, S., "The Scattering of X-rays by Interstellar Dust on the Micro-Arcsecond Scale", *Ap. J.,* **528**, 306-309, 2000.
- Cash, W., Shipley, A., Osterman, S., and Joy, M., "Laboratory Detection of X-ray Fringes with a Grazing-Incidence Interferometer", *Nature*, **407**, 160-162, 2000.

- Cash, W., White, N., and Joy, M., "The Maxim Pathfinder Mission: X-ray Imaging at 100 Micro-Arcseconds", ASP Proceedings, **234**, <u>X-ray Astronomy 2000</u>, 619-626 2001
- Cash, W., "X-ray Interferometry", IAU Symposium 205, <u>Galaxies and Their Constituents at the Highest Angular Resolutions,</u> Schilizzi et al editors, ASP Press, 457-462, 2001
- Cash, W., Shipley, A., and McEntaffer, R. L., "X-ray interferometry: ultra-high-resolution astronomy", *Proc. Soc. Photo-Opt. Instr. Eng.*, **4506**, 127-135, 2001.
- Shipley, A., and Cash, W., "Alignment of a Grazing Incidence X-ray Interferometer", *Proc. Soc. Photo-Opt. Instr. Eng.*, **4444**, 17-28, 2001.
- Cash, W., White, N., and Joy, M., "The Maxim Mission: X-ray Interferometry in the New Century", ASP Proceedings, **251**, <u>New Century of X-ray Astronomy</u>, 206-209, 2001
- Several more papers are to be presented at the SPIE meeting in Hawaii in August 2002.

Publicity:

The Goddard publicity office prepared a press release about x-ray interferometry and Maxim and released it in conjunction with the Nature articles. This made a very big splash worldwide. It appears that there are lots of people who are excited by the potential of "Ultimate Astronomical Imaging". I think the exposure we received will help make the interferometry a reality.

- http://www.msnbc.com/news/SPACENEWS_Front.asp
- http://www.discovery.com/news/briefs/20000913/te_sp_megascope.html
- http://news.bbc.co.uk/hi/english/sci/tech/newsid_924000/924684.stm
- http://www.space.com/scienceastronomy/astronomy/new_xray_scope_000913.html
- http://dailynews.yahoo.com/h/ap/20000913/sc/black_hole_telescope_1.html
- http://www.flatoday.com/space/explore/stories/2000b/091400a.htm

B. Simulations

An important question that needs to be answered for x-ray interferometry is what science it will be able to achieve. Simulating the types of objects that the interferometer is likely to see, while also taking into account instrument specifications, can provide a solution. Figure 9 displays point sources with a variety of characteristics as seen through an array of 32 flat mirrors arranged in a ring. Figure 9 shows the probability distribution function (PDF) for a 1keV point sources. The next three images show Poisson data generated using the corresponding PDFs.

Other interesting simulations using point sources include those depicted in Figure10. These are a series of binary systems with differing intensities and separations in the same field of view. In Figure 10 a the central source has flux half that of the source that is displaced to the lower left. The next image shows 9000 total events for this system with the lower flux source having twice the intensity of the higher flux source. Even though the higher flux source is in the first maximum of the other, the two can be easily distinguished. Following this is another image with 9000 events. However, this time the central source has five times the intensity of the higher flux source and now the presence
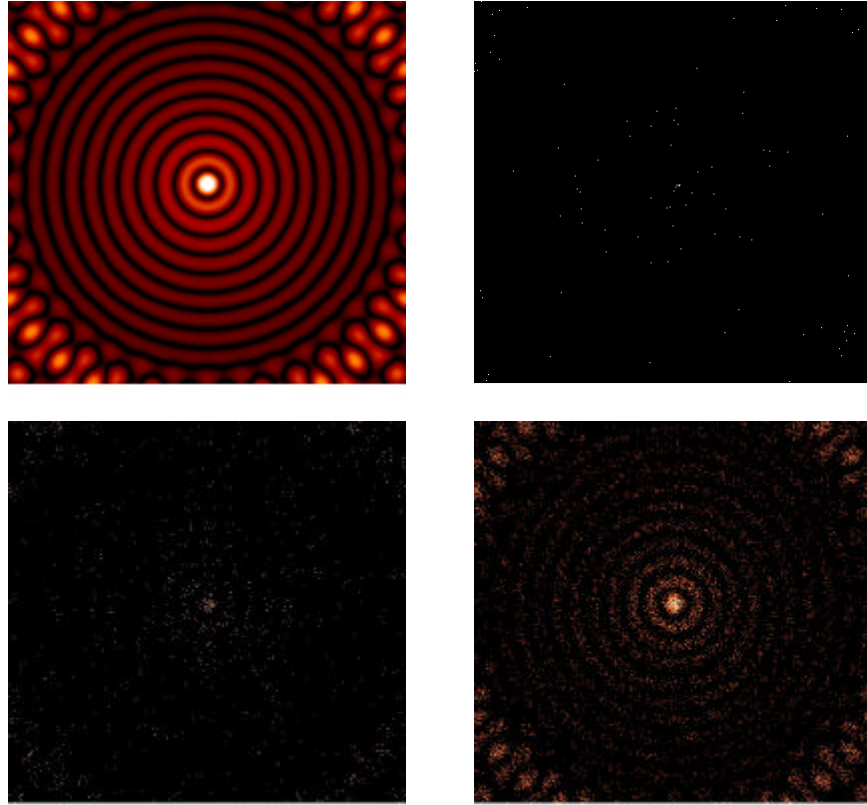
Figure 9: Simulations of point sources viewed by a 32 mirror interferometer. a) beam pattern at 6keV b) beam pattern at 1keV c) poisson data simulated at 6keV d) data at 1keV e) beam pattern of 0.5 to 6keV continuum f) data simulation of continuum

of a second source is not obvious. Figure 10d shows the same system with a smaller separation so that the higher flux source is in the first null of the lower flux source. Now, the higher flux source is noticeable not only at half the intensity but also at a fifth of the intensity of the lower flux source.

A series of simulations more indicative of MAXIM's capabilities is shown in Figure 11. These images depict how stellar coronae would appear to MAXIM. The first image is a SOHO image of the Sun in the extreme ultraviolet. This is probably analogous to the high altitude regions of many solar type stars in our vicinity. The image was sensitivity limited to the pixels with the highest count values.
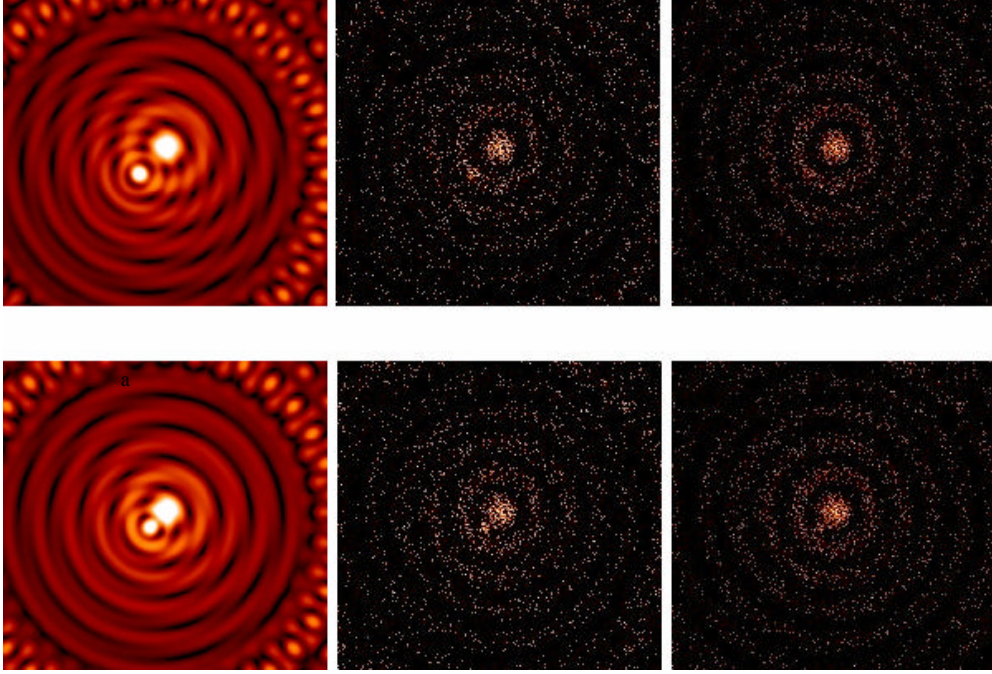
Figure 10: Binary point source distributions at differing intensities and separations. These simulations demonstrate that the interferometer acts like a telescope with major diffraction rings.

A new image was made by mapping a point source to the position of each pixel that contained a value. The intensity of each point source was scaled according to the pixel's count value. The result is shown in Figure 7b. This probability distribution function was then used to define the mapping of Poisson data as shown in the final image.

a   b   c
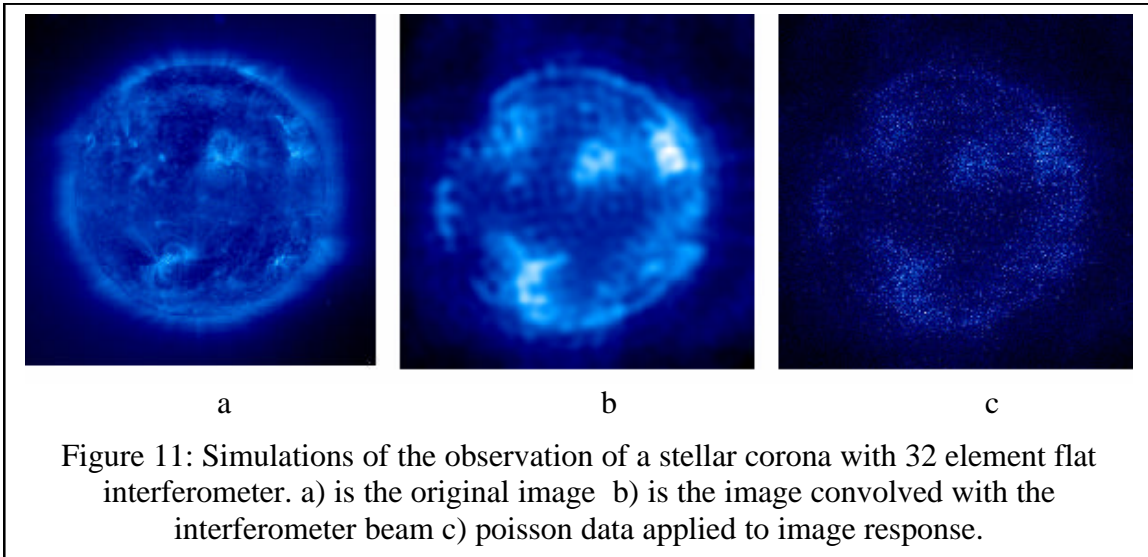
Figure 11: Simulations of the observation of a stellar corona with 32 element flat interferometer. a) is the original image b) is the image convolved with the interferometer beam c) poisson data applied to image response.
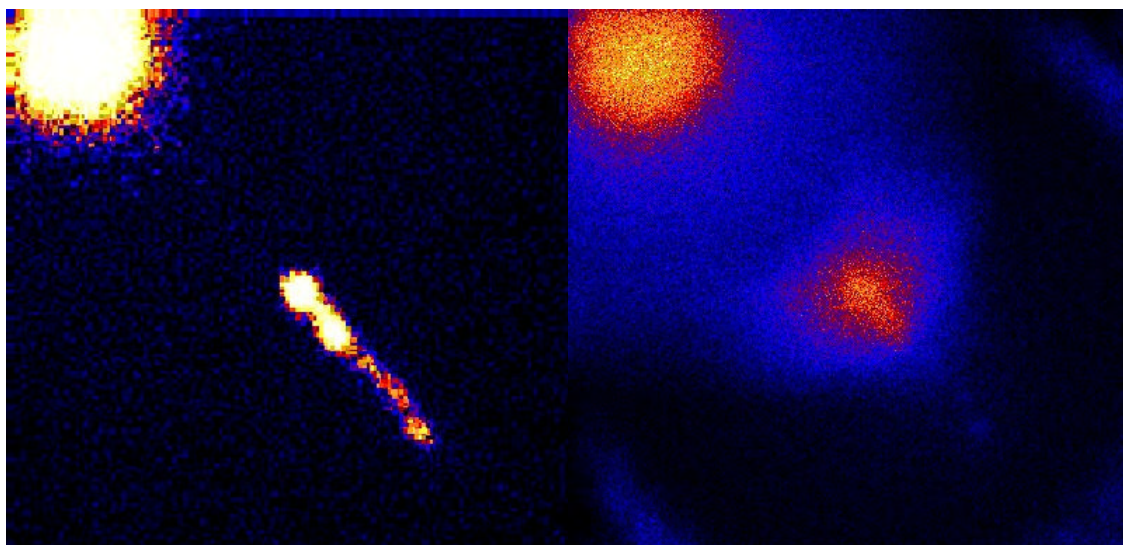
Figure 12: Simulation of observation of an AGN jet. To the left is the Chandra image of the quasar 3C273. To the right is the image convolved through an interferometer point response function, showing that the basic features are not hidden by the beam pattern.

C. Periscopes

By the second year of the Phase II study we had developed a detailed understanding of not only the architecture of the x-ray interferometer, but also of all the tolerances that drive the design. These tolerances were reported in Shipley et al 2001. As our understanding of the tolerances grew more sophisticated, an alternative configuration was invented that has major advantages in solving the difficulties in the components of the architecture. Here we give a preliminary account of the modified architecture. The details will be forthcoming in the next set of publications.

The idea was to move the pairs of flats into close proximity as shown in Figure xxx. Two parallel flat mirrors reflecting light in sequence are, of course, known as a periscope. In our case we make the mirrors almost, but not exactly parallel.

To focus

ψ

Parallel to Source Direction
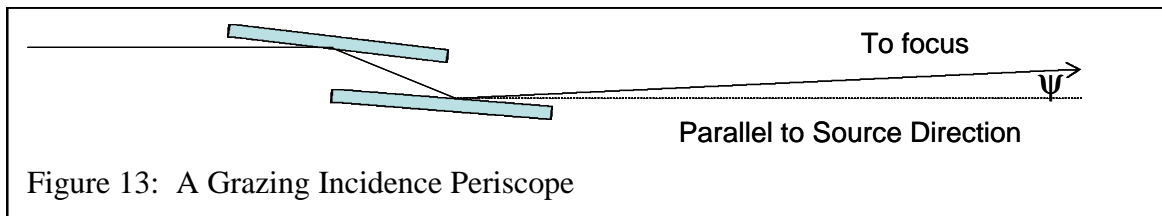
Figure 13: A Grazing Incidence Periscope

This creates a slowly convergent beam with a very long focal length. It is, in essence, a thin lens, and has many of the attractive features of a thin lens.

21

First, the periscope configuration has a wider field of view (see attached Ball studies). The "X Configuration" was limited to a modest field by a severe comatic aberration. The field of view of a periscope system can be very wide – over an arcsecond at micro-arcsecond resolution.

Second, because the baseline sensitivity of our grazing arrays scales as the angle at which the beams converge, the periscope has full, nanometer class sensitivity within the periscope only. Each periscope must be in position held to $\lambda/(20\sin\psi)$, where ψ is the convergence angle toward the focal plane. Since ψ is closer to one arcsecond than one degree, the periscopes only need to be held on the baseline to a tolerance of microns, rather than nanometers. This will greatly ease the fabrication of the arrays.

Another advantage that comes with the periscope system is the built-in delay line. In the x-configuration all the mirrors are close-packed and set in a ring that by symmetry creates equal path lengths through each channel. However, as is well exemplified by the VLA, a high quality interferometer array samples a variety of frequencies. This requires periscopes be placed at different distances off axis. Unfortunately, that means that the central rays reach the focal plane with a shorter path than those from the outer parts of the array. The periscopes provide a natural delay line. By placing the mirror pairs in the central periscopes a little bit farther apart, the required delay is achieved with no noticeable effect on the array.

Figure 14: Because each periscope can act as a delay line, the components of the interferometer array can be stationed at many radii and sample more of the UV plane.
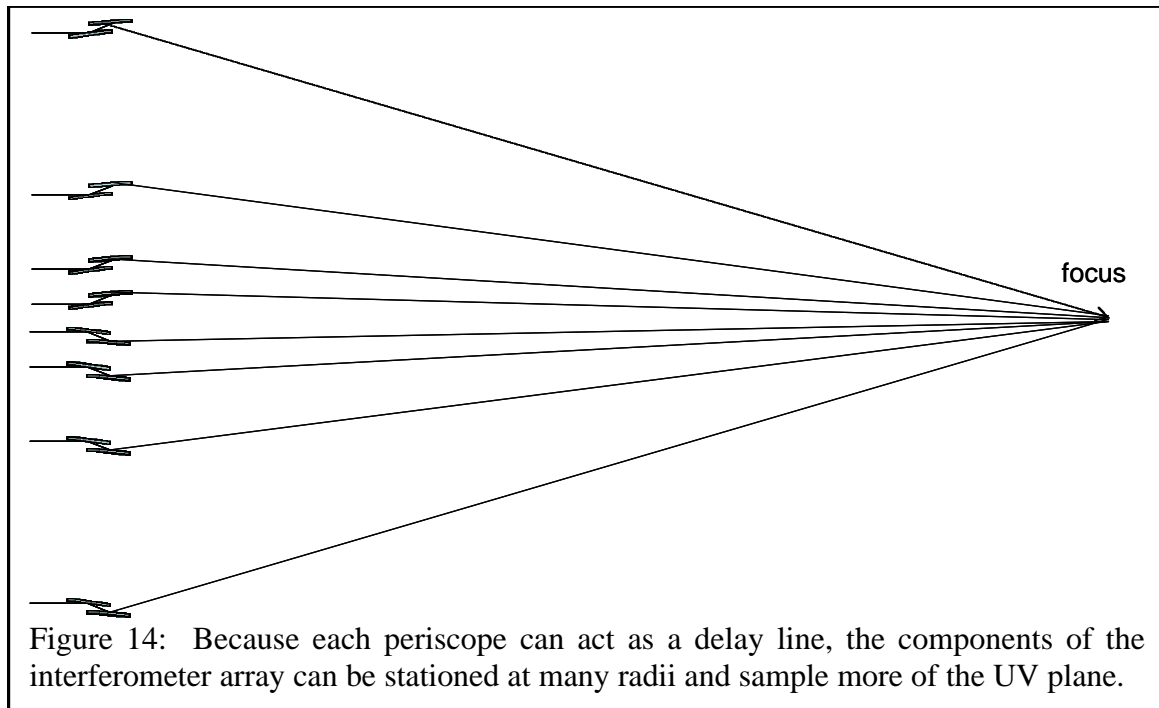
Another tremendous advantage of the thin lens aspects of the periscope array is the relaxation in pointing requirement. If a thin lens shifts its aspect with respect to a target, the position of the focus does not move. If we hold the detector on the line of sight to the source, the image will not move as the interferometer pointing wobbles, greatly reducing the required stability of the optics craft.

But this leaves us with what we now call the "Line of Sight" problem. Information about the line of sight from the detector through the center of the interferometer to the celestial sphere becomes the main problem. Because the field of view is huge, we only need stability to keep the image on the detector and information to correct the position of each recorded photon.
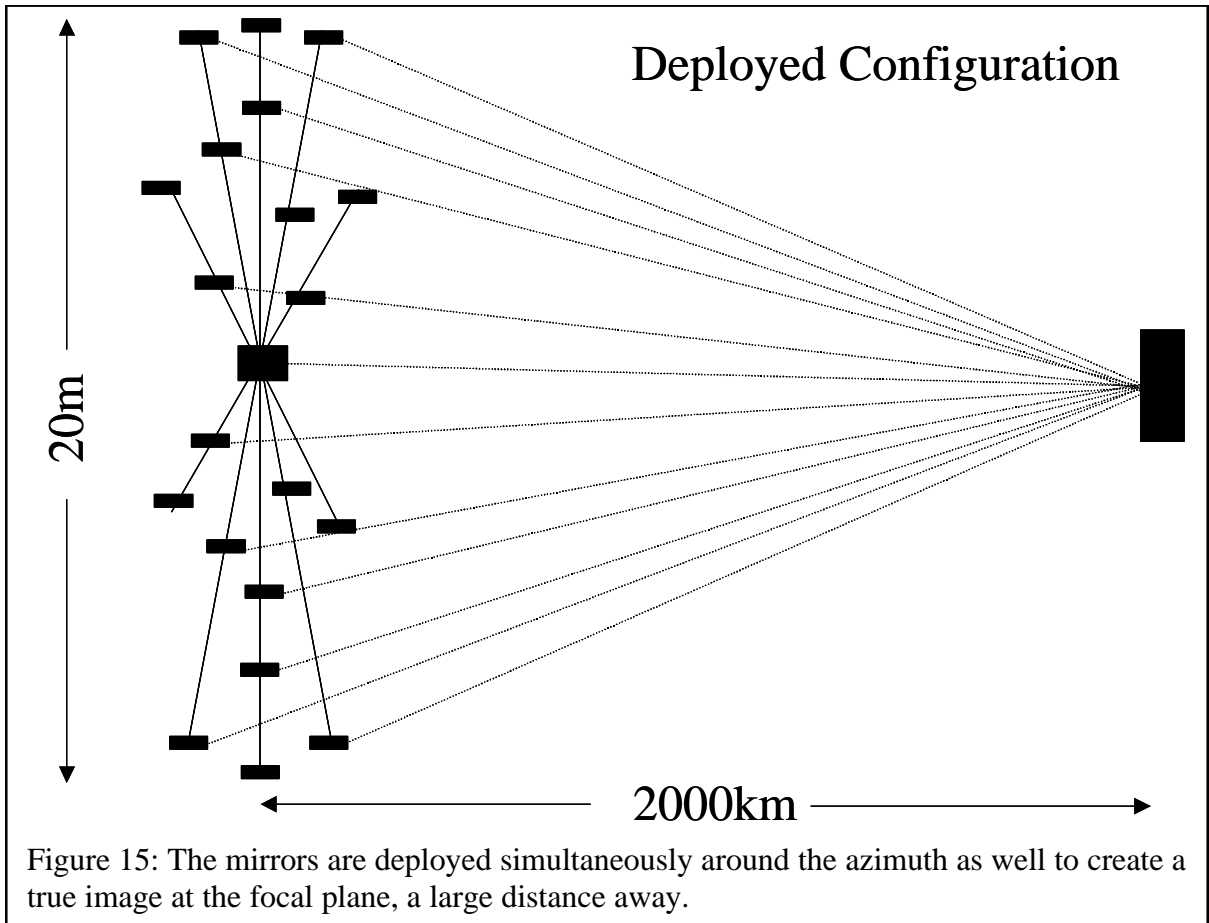
Figure 15: The mirrors are deployed simultaneously around the azimuth as well to create a true image at the focal plane, a large distance away.

However, this is the most difficult remaining task. We have to get the knowledge to about 5 microns at distances from 200km to possibly as high as 20,000km. Actual stability of the detector craft is much more forgiving. Basically we have to keep the image on the detector – absolute position of millimeters or even centimeters. It's the 5µ knowledge that's the problem.

Two solutions are under development. The simplest conceptually is to double-up the interferometer array. One interferometer will observe blazars or other bright celestial x-ray sources to create a stable line of sight in space. A second detector craft will observe it and relay stability of the interferometer information to the first detector craft. This will solve the problem, but it is awkward and expensive.

A more elegant and general solution to the problem is under development by Dr Keith Gendreau at Goddard Space Flight Center. He has dubbed his solution the "super-startracker", and it may have application to more than x-ray astronomy. However, it is beyond the scope of this report.

V. Laboratory

During the period of this study we have made progress in the laboratory. This is best exemplified by the paper in *Nature* demonstrating fringe formation.

Modeling

One major activity of this program is the modeling and simulation of the mission performance. This is relevant to mission architecture, in that it helps set specifications, but its primary function at this early stage is to communicate the power of the observatory in a quantitative and convincing fashion. A variety of activities are going on in this area.

We need further simulations of the data analysis – the inversion of the fringes into 2-D images. We used our lab interferometer to obtain fringes of a slit at different azimuthal angles. We first tried the famous ART algorithm that was initially used for CAT scans in the early 1970's. We found that it failed to properly reconstruct high frequencies. We next tried a version of CLEAN, the approach favored by radio astronomers. This worked nicely, creating Figure 16.
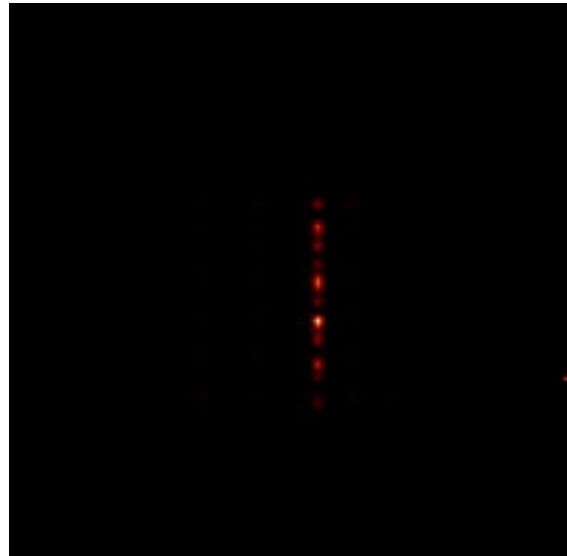
Figure 16: A reconstructed image of a slit taken in the laboratory with the x-ray interferometer. Wavelength = 304Å.
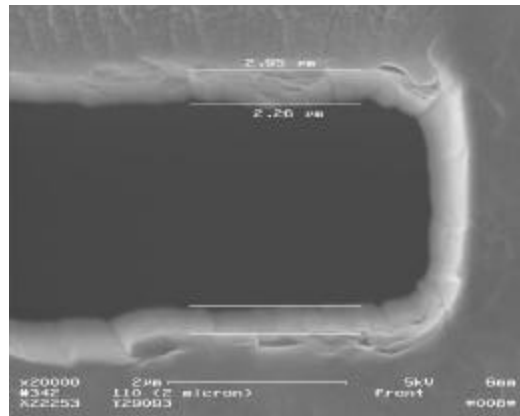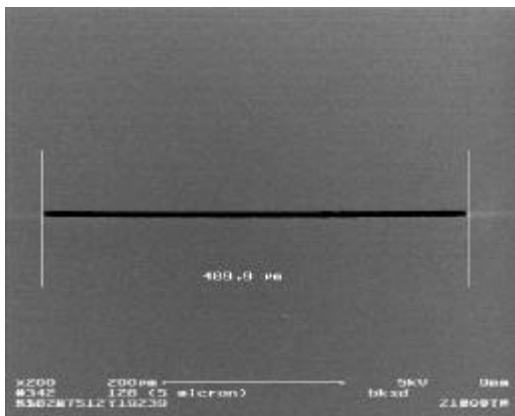
Figure 17: Photomicrographs of high precision slits.

We had to use some (somewhat suspect) shortcuts on this first image, but it gives one confidence that the systems work. The bumpiness along the length of the slit appears to an artifact of the setup. We intend to try fourier inversion and maximum entropy next.

Slits

Another small side effort that was supported by this study was the fabrication of very thin slits. Performed at MIT, we had some sub-micron slits fabricated. They will become of central importance to the calibration of the x-ray interferometers as they will allow us to demonstrate high resolution performance in much shorter calibration beamlines. Figure 17 shows electron micrographs of the fabricated slits.

VI. Ball Study

Much of the effort centered on Ball's use of their proprietary integrated mission design software. This software allows one to simulate all the behaviors of the components of a spacecraft and understand their impact on the scientific data. Ball built a complete model of both mission levels – the pathfinder and the black hole imager. Investigations with the integrated approach gave us some confidence of success. Although x-ray interferometry is very demanding, it appears that the superstructure of the Ball software is sufficiently flexible to meet our needs. Ball is currently using the code to create a full model of the Next Generation Space Telescope (NGST) and the interferometric extension of the Very Large Telescope (VLT).

Some of their results for the NIAC study are found in the following two appendices.

Appendix 1: Ball Optical Study of Periscope Configuration

The periscope Pathfinder optical sensitivities are derived for a 1.400 meter baseline design. Figure (1) shows a diagram of the X-ray telescope system that was analyzed. There are 32 mirror pairs. The first group of 32 mirrors are located on a ring that is 1.4 meters in diameter and are equally spaced rotationally at an angle of 11.25 degree to each other. The mirrors are 3X83 cm and rotated to the incoming beam so that the xrays strikes each mirror at 2 degree graze angle. The second group of 32 mirrors are located on a diameter of 1.335668 meters and are located with their centers 46 cm behind the first group of mirrors. These mirrors are also rotated so the light from the first mirror group strikes the second mirror group at a 2 degree graze angle. There is a slight increase to the rotation of the mirrors in the second group. Rather than having the X-rays exit the second mirror group parallel to the incoming X-rays (like a Periscope) the x-rays leave the second mirror group at a very slight angle towards the optical axis of the system. The angle is set so the X-rays "focus" 400 km away on the detector. This small change in angle is only 0.172 arc-seconds less than 2 degrees.
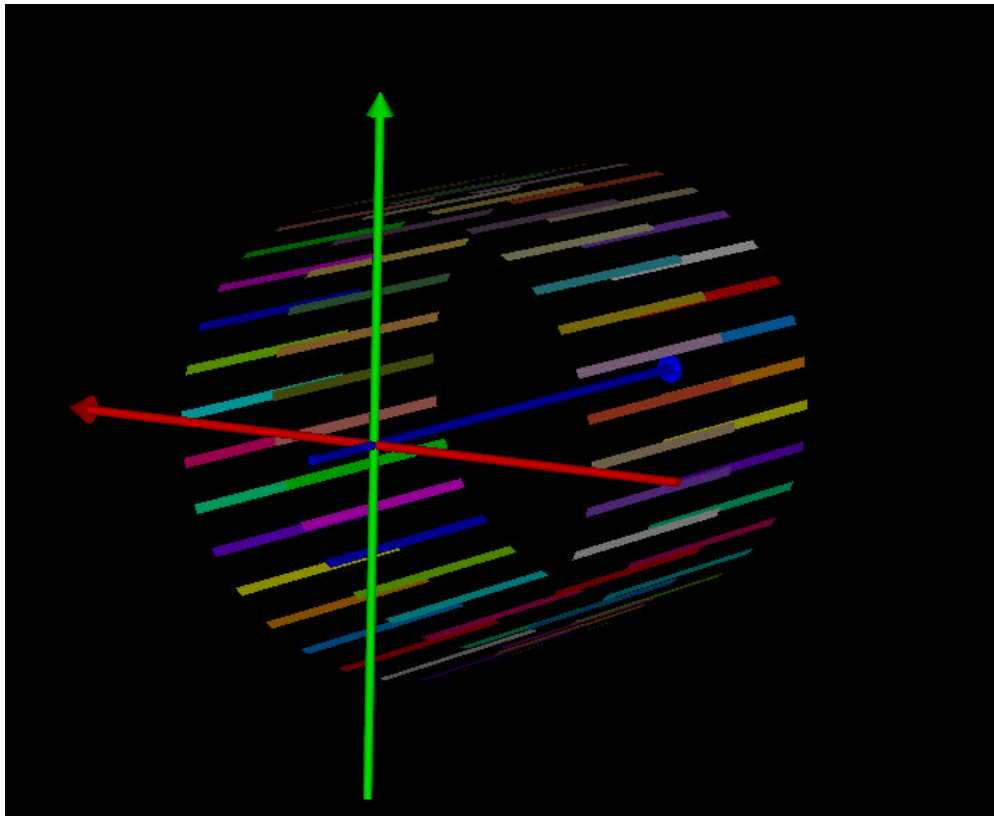
Figure(1) 32 mirror pair periscope X-ray telescope 1,4 meter baseline. X-rays enter from the left and are reflected towards the +Z axis (Blue). The detector is located on the +Z axis 400 km away

Figure 2 shows a diagram of one of the 32 mirror pairs in Figure 1. The mirrors are located such that the center of the first mirror in above the edge of the second mirror.

1 mirror pair of Periscope Telescope

2°-(4.7830087E-5)

To detector

Y

Z

From X-ray source

2°
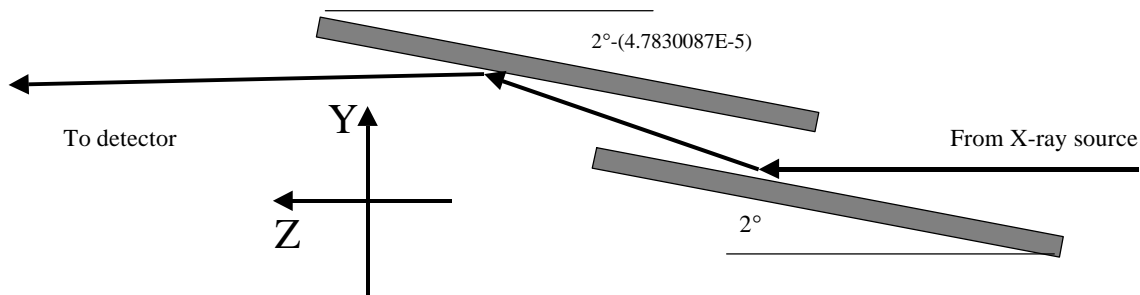
Figure 2 Diagram of a mirror pair in the Periscope X-ray telescope

An optical sensitivity analysis was done for this system. This involved applying random rotation and position errors to each of the 64 optics in the x-ray telescope. The coordinates for how errors are applied is shown in Figure 3 which shows a single optic.

Towards optic axis

Reflective side for 1st optic group and backside of optic for 2nd optic group.

To detector

Y

From source

Z

X
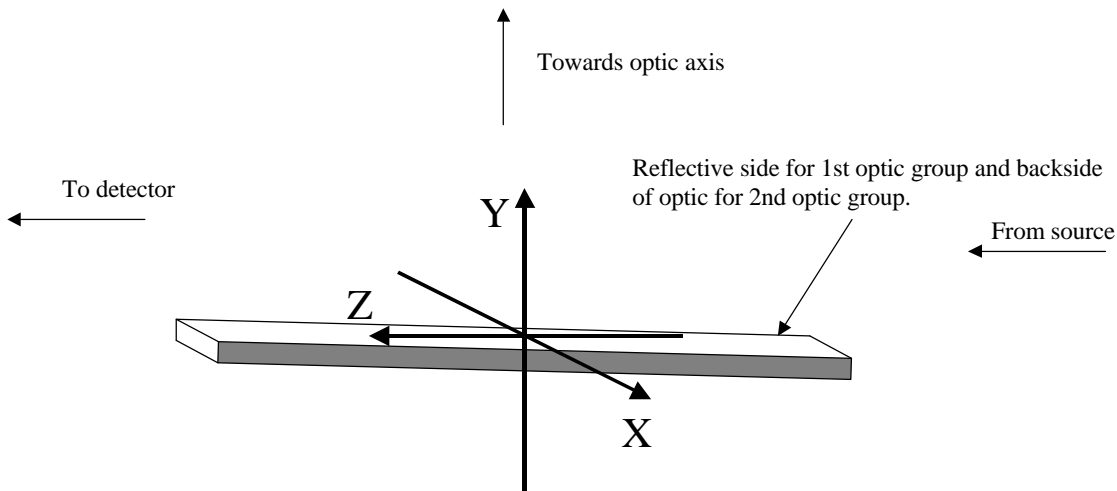
Coordinate system local to optic

Figure 3- Coordinate system for applying optical errors. The optic is tilted to the coordinate system by 2 degrees. Tip tilts and displacements are applied in the global coordinate system using the axis as shown.

The system sensitivities to Radial, and axial Z optic position errors are derived. From Figure 3, X position errors have no effects on optical wave front quality and only effects the clear aperture. The system sensitivities to X, Y, and Z rotation errors are derived.

A Monte Carlo approach was used to derive the optical sensitivities. Only one error source was varied at a time. A uniformly random error was generated where a given tolerance set the maximum and minimum values of the random distribution. Five runs where performed for each tolerance and the average of the runs was summed to derive the effect of the tolerance. The tolerance for each error type was also varied to derive a system sensitivity curve to that error source. The criteria for analyzing the effect of the errors are the Strehl ratio. This is defined by the peak intensity from a point with the perturbed system divided by the peak intensity of a point source with a "perfect" system with no errors.

Figure 4 shows the sensitivity to Radial de-space (Y-despace) errors. This error can be thought of as random movement in the radial direction for each of the 64 mirrors. The system is quite sensitive to these errors where a tolerance of < (±20Å) is required to keep the Strehl >80%. The plot stops at errors greater than 60Å because most of the 5 runs did not show a central maximum with radial errors greater than 60Å.
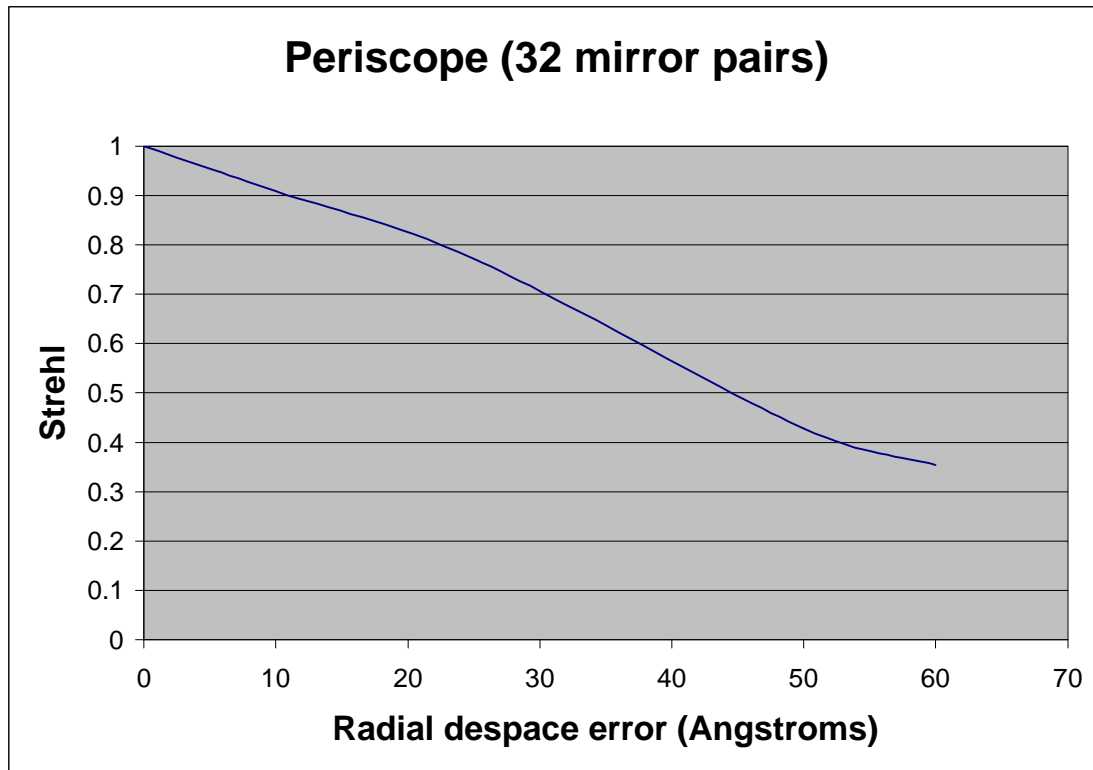
Figure 4. Y de-space error sensitivity

Figure 5 shows the sensitivity curve for Axial de-space (Z-de-space) errors. This error can be thought of as random movement in the axial direction for each of the 64 mirrors. The system is not as sensitive to these errors where a tolerance of < (±.07 µm) is required to keep the Strehl >80%.
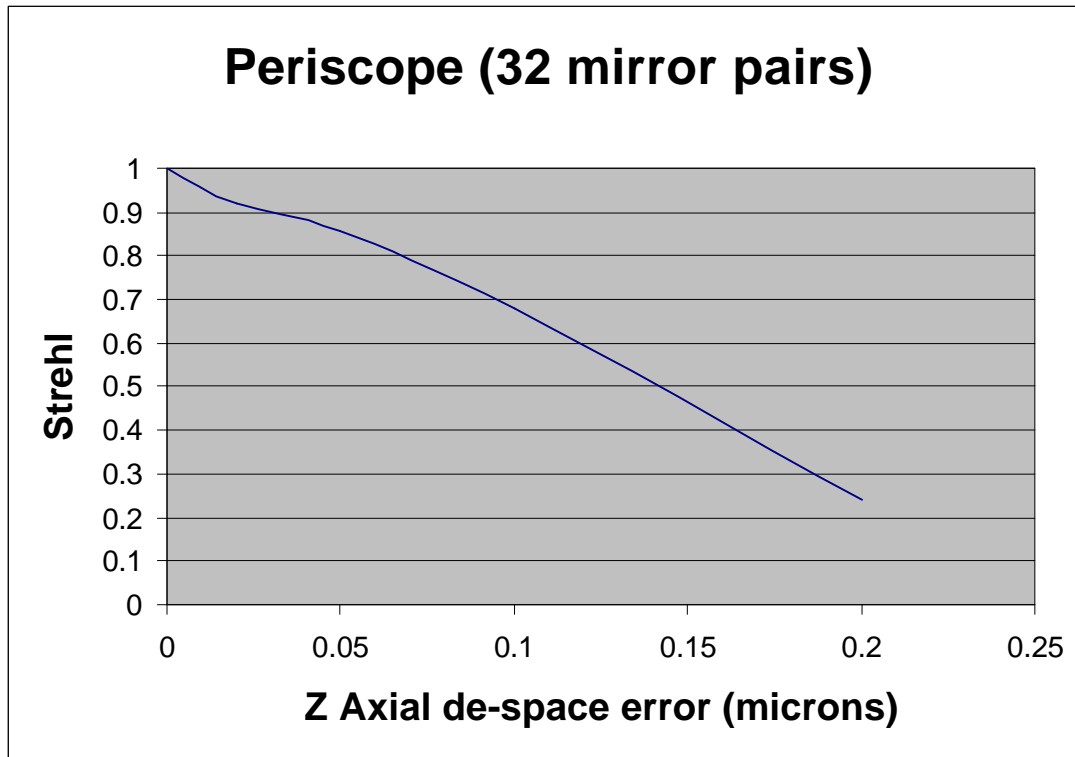
Figure 5 Sensitivity to axial de-space errors

Figure 6 shows the sensitivity to X-axis rotation errors. This error can be thought of as a random variation in the 2 degree graze angle. The system is extremely sensitive to these errors where a tolerance of < (±.002 arc-seconds) is required to keep the Strehl >80%.
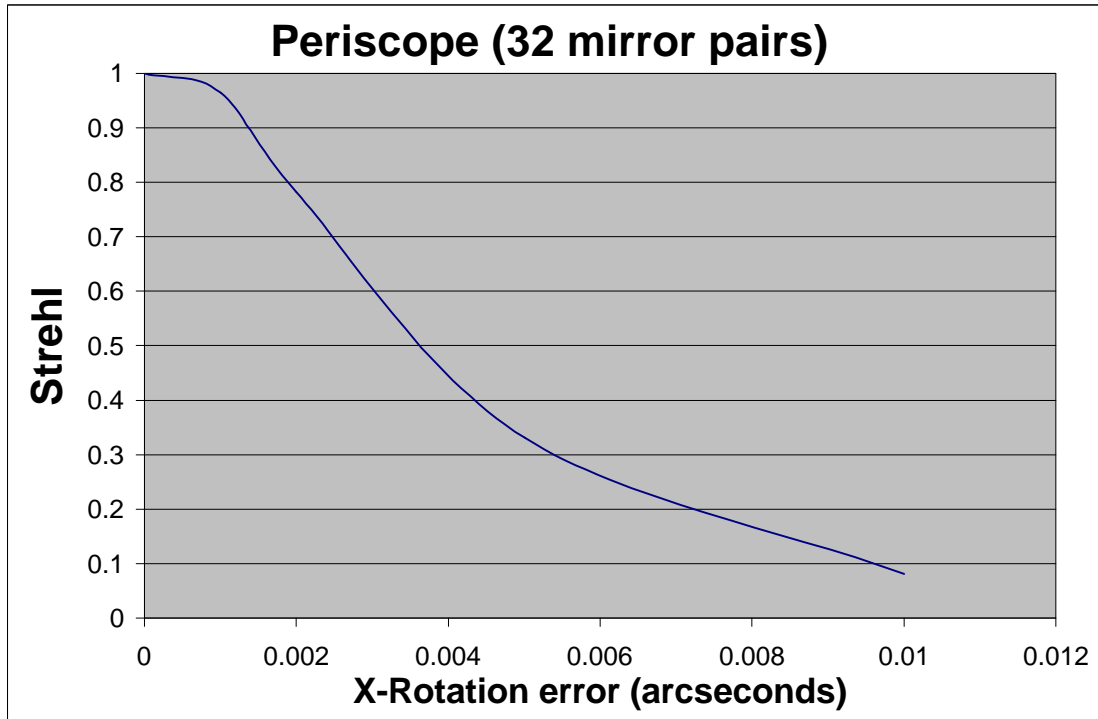
Figure 6 X-axis rotation error.

Figure 7 shows the sensitivity to Y-axis rotation errors. This error can be described by taking a single optic and balancing it on you finger against the optical surface. Put a 2 degree tip to the optics. Now take the optic and rotate it in random direction. The system is not very sensitive to these errors where a tolerance of < (±1.7 arc-seconds) is required to keep the Strehl >80%.

Periscope (32 mirror pairs)
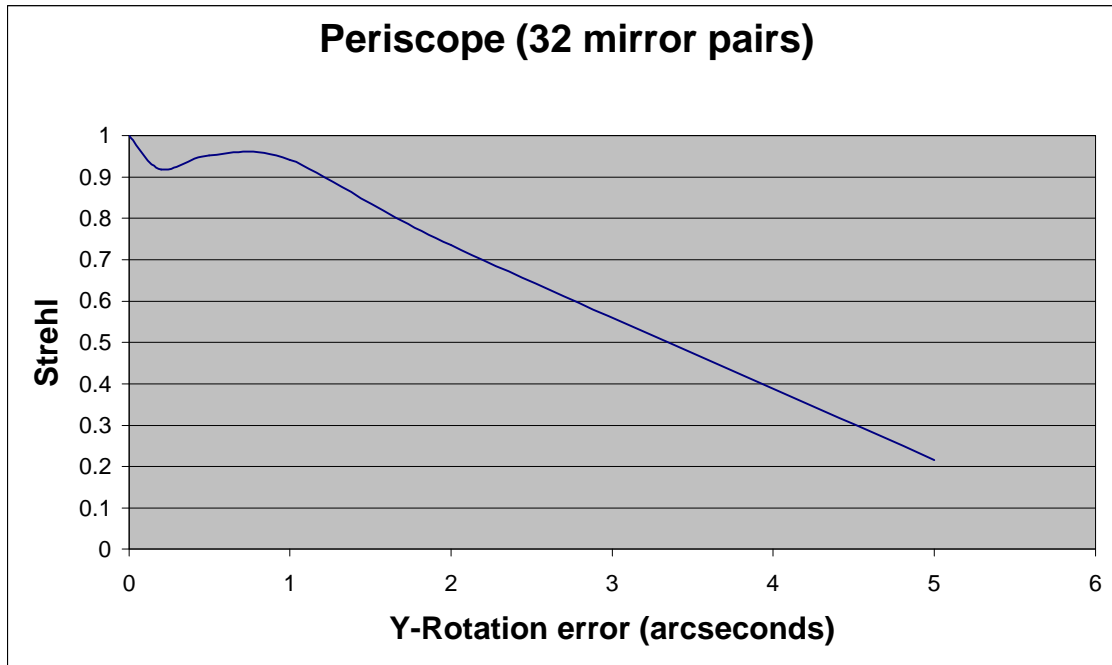
Figure 7 Y rotation errors. The slight dips in the 90% range may be due to insufficient averaging or aliasing with the apertures sizes and rays numbers in the software.

Figure 8 shows the sensitivity to Z-axis (optical axis) rotation errors. This error can be described by taking a single optic holding it on the short sides in the long direction of the optic. Put a 2 degree tip to the optic. Now take the optic and rotate it in random direction. The system is moderately sensitive to these errors where a tolerance of < (±.06 arc-seconds) is required to keep the Strehl >80%.
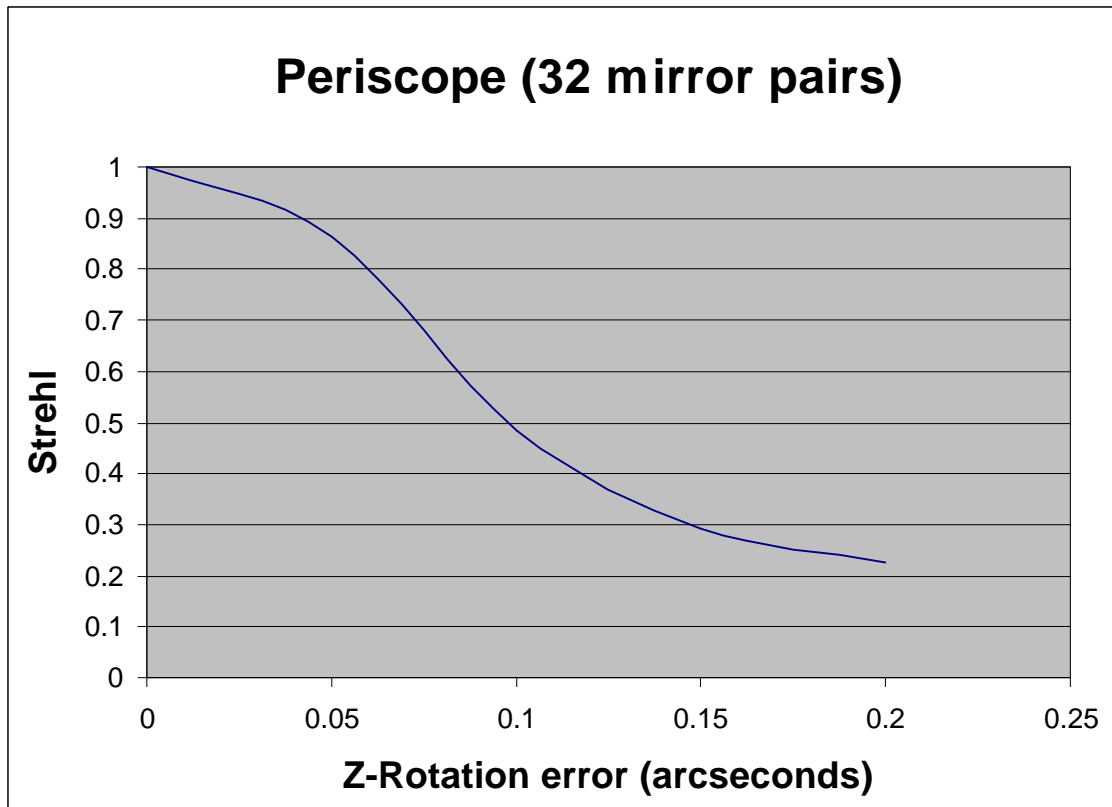
Figure 8 Z rotation errors.

Encircled Energy Analysis

Figure 9 shows an image with the periscope x-ray telescope. 90% of the energy is contained inside about a 30 mm diameter circle. The next plot in figure 10 shows the encircled energy.
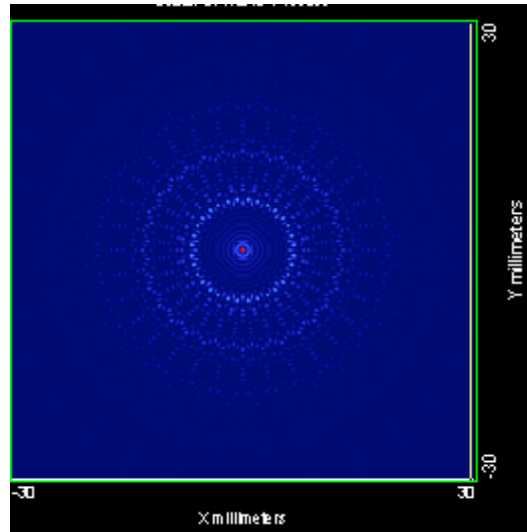
Figure 9 (top) A close up of the central 5mm of the image and (bottom) a full view of the 30X30mm image.

RADIAL
PERCENT
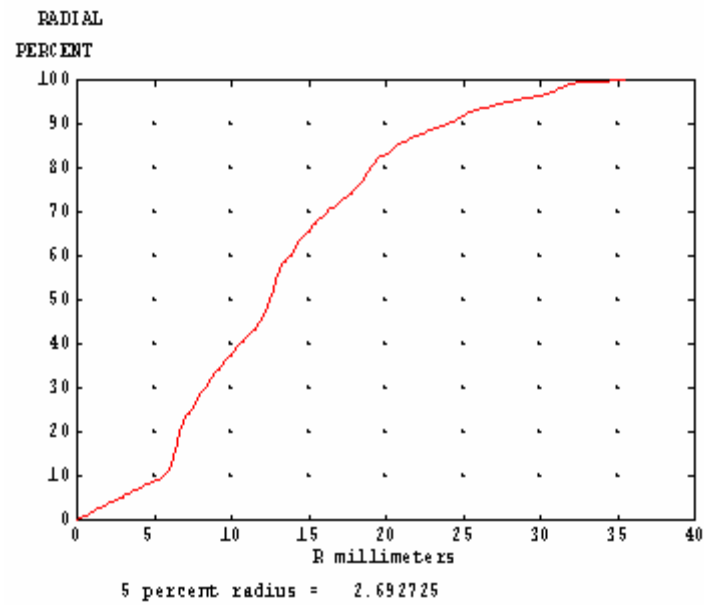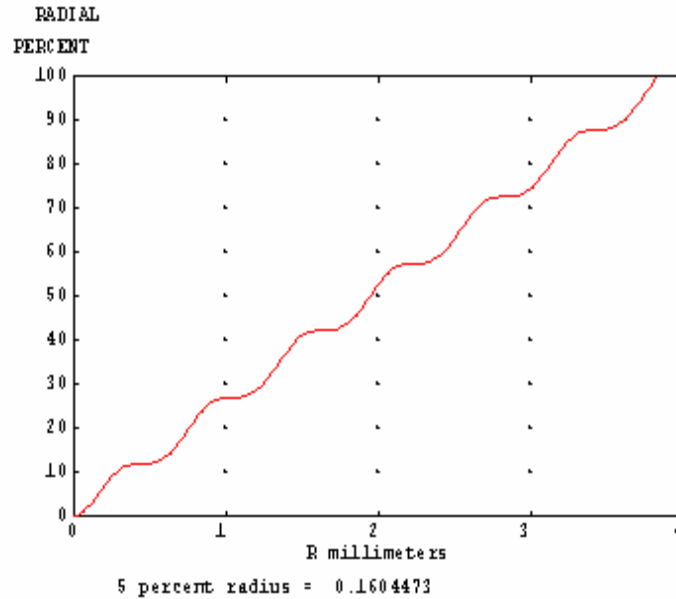
Figure 10 The top figure shows the encircled energy of the full image from the x-ray telescope. Note 5% of the energy is inside a radius of 2.6927 mm. The next plot shows a close up of the central region of the image where ~70% encirlced energy is scaled to 5% encircled energy at 2.6927 mm. So the plot should be scaled by ~(5/50) to give the encircled relative to the full image. **Only about 1% of the energy is contained in the central first dark ring for a perfect system with an on-axis point source.**

System Tolerances

To set a minimum requirement for a X-ray periscope system it seem reasonable that the Strehl ratio should not be allowed to fall below 50%. The tolerances need to be weighted according to the difficulty in achieving them. Clearly the Y rotation tolerance should be held to much less than an arc-second so its contribution has effectively no degradation to the system Strehl. Figure 11 shows an error budget allocation to the system Strehl to yield a 50% system Strehl. The budget was broken down into equal degradation of the Strehl comes from mirror tilts error and from mirror de-centers errors. Note optical figure errors are not included in this calculation.
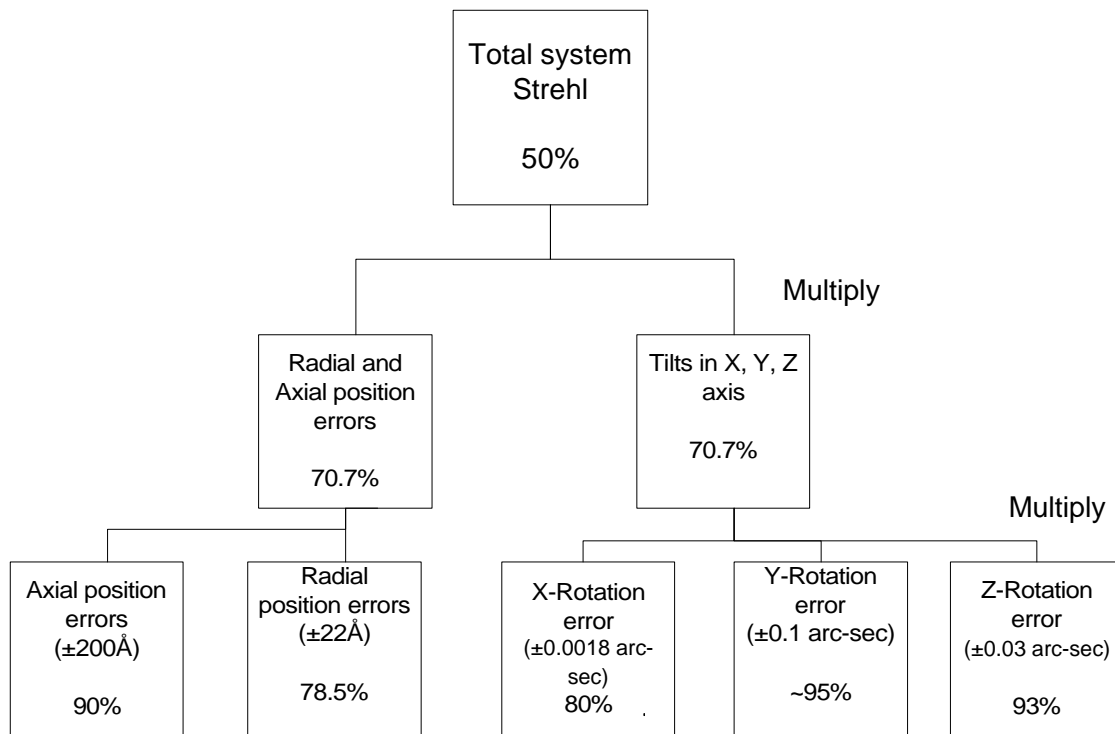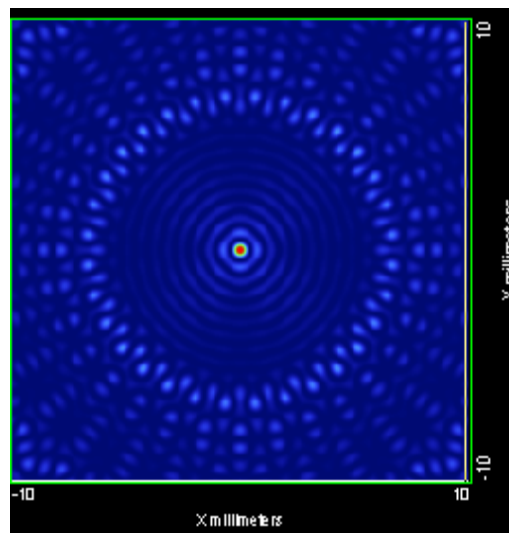
Figure 11 Error budget tree for 50% system Strehl with the 32 mirror pair periscope x-ray telescope.

Figure 12 shows three images with the 32 mirror periscope system with the errors from Figure 11 applied to the telescope mirrors in a uniformly random fashion. The top image is the telescope with no errors.
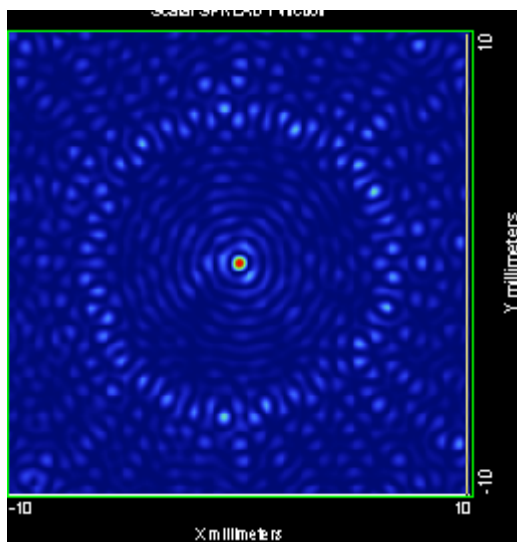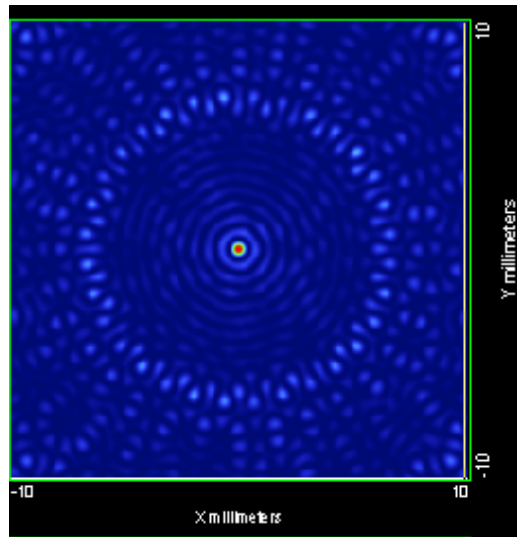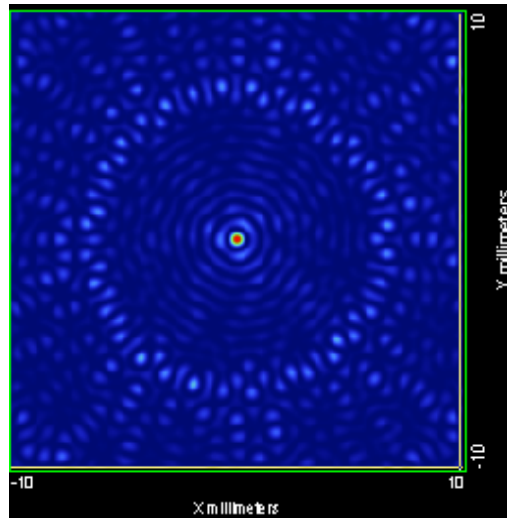
Figure 12 : Three images with the 3 mirror periscope system. The images are from three runs with the errors shown in figure 11 applied in a random fashion to each optic. The top figure is the telescope without errors. The field is 5.2X5.2 milli arc-sec. The average Strehl came out a better than expected from the error budget @ 73.3%.
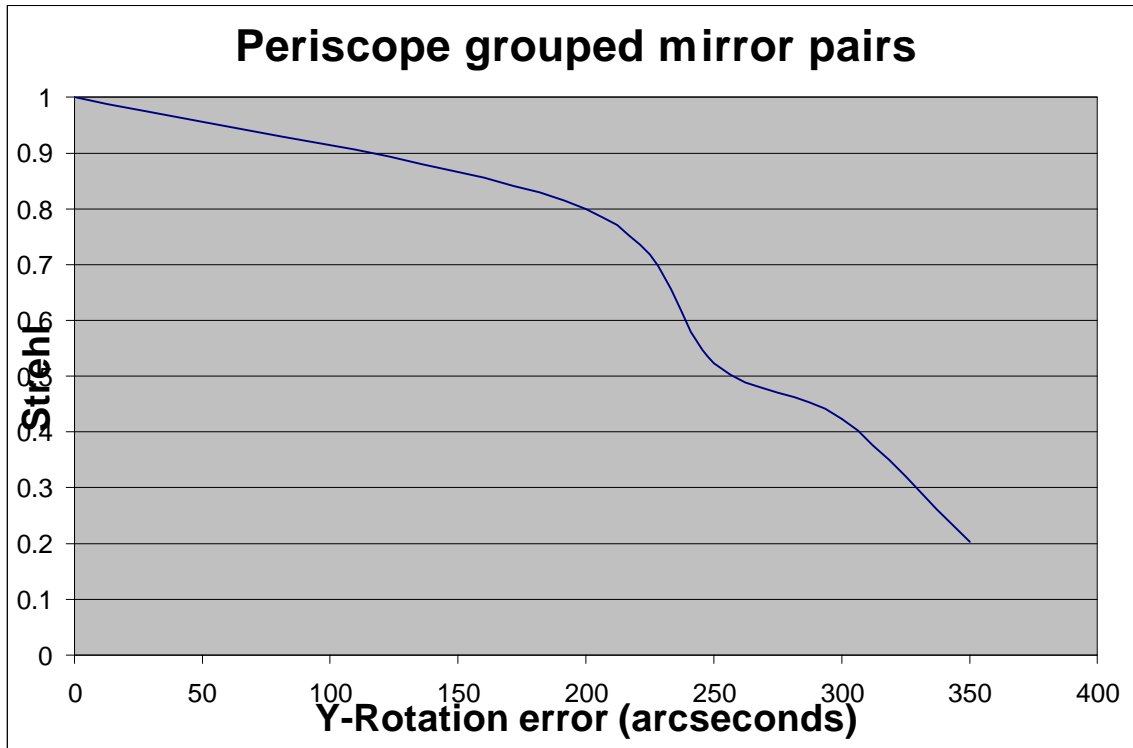
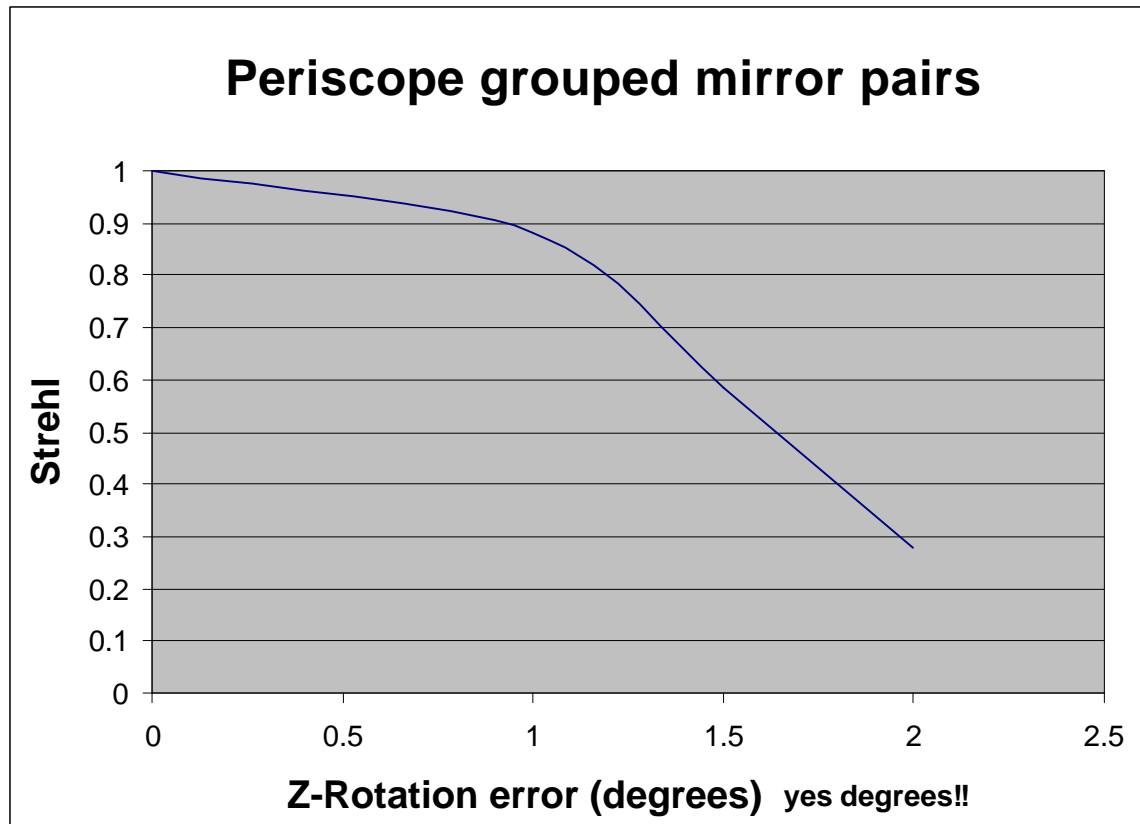## Tolerance analysis using mirror pairs

Each front and rear mirror pairs were group and randomly moved together in tilts and de-centers. The coordinate system used is shown in figure 2. The center for the rotations is the geometric center of the mirror pair. This point is centered between the mirrors in both the radial and axial positions. Not the pupil for each optic was fixed so the large motions and tilt could have some aperture effects.
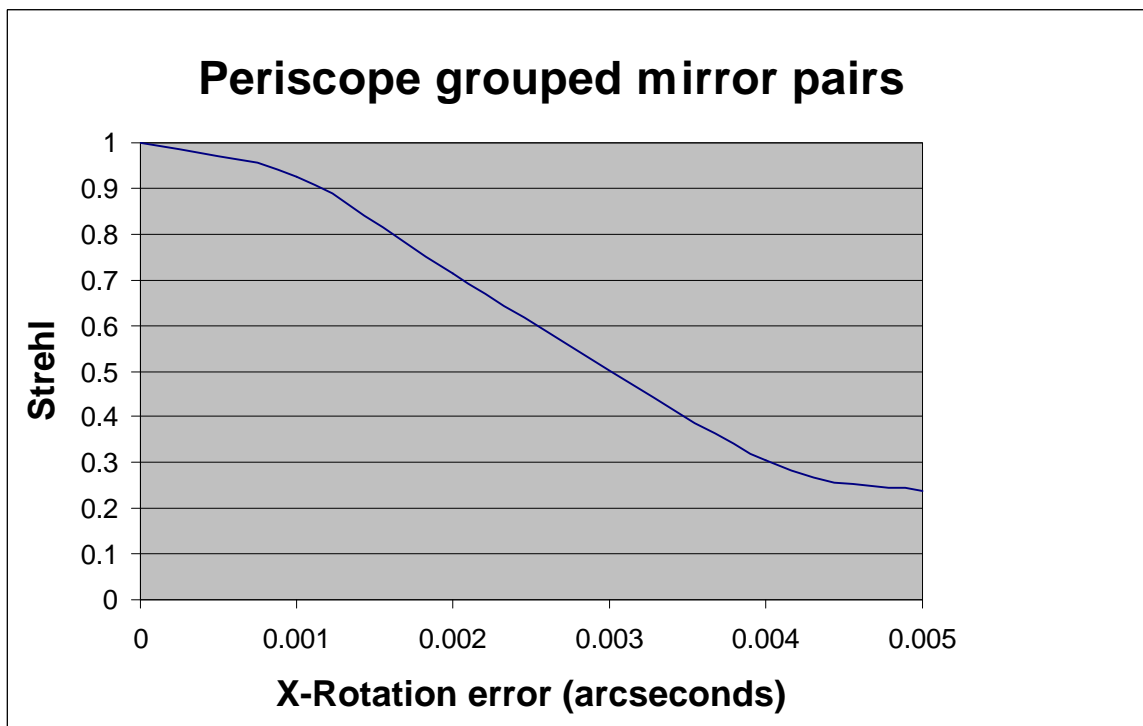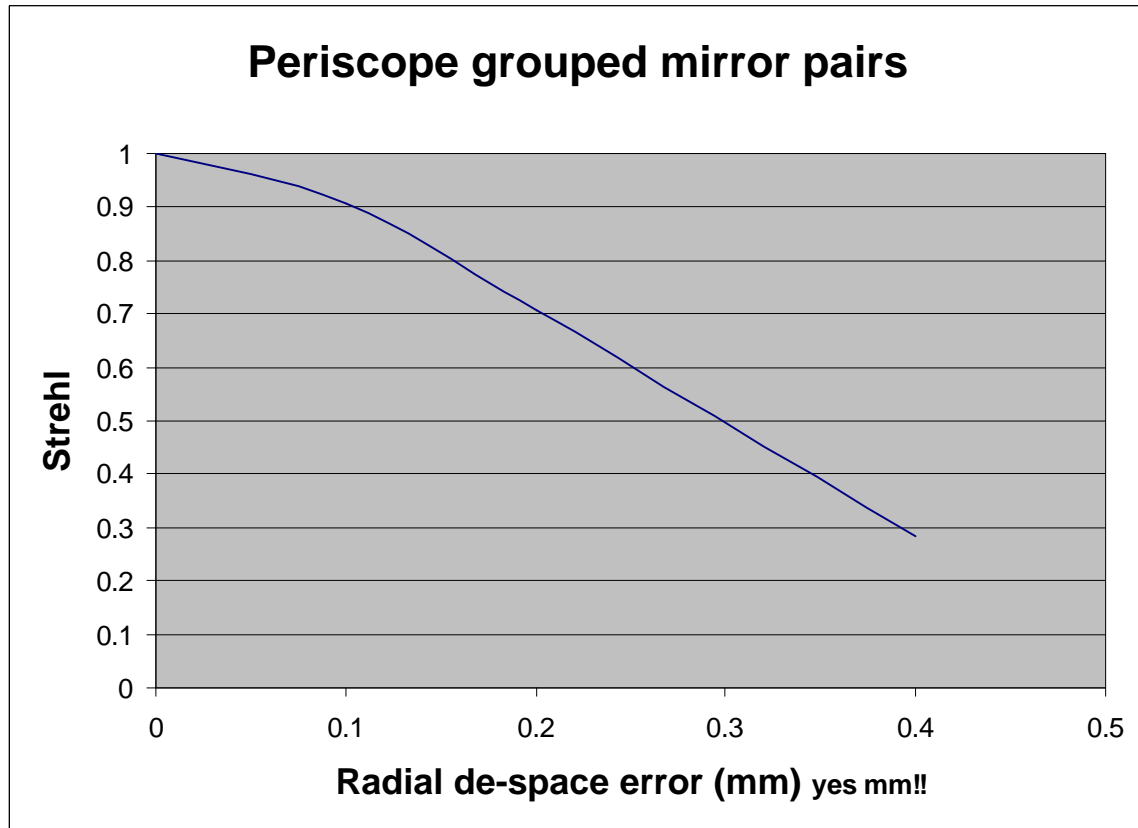

Seems we don't have decreased sensitivity in the X-axis as we thought the periscope should. I think lateral motion of the fringes at the focal plane is what is making this motion so sensitive. The flattening of the curve after .004" is probably due to poor averaging in my runs. In some cases the spot was not clear

so I could not compute a Strelhl, this would skew the data higher since I would be sampling the "good" random runs only.

Periscope grouped mirror pairs

Y-axis: Strehl (0 to 1)
X-axis: Y-Rotation error (arcseconds) (0 to 400)

Periscope grouped mirror pairs

(Y-axis: Strehl, ranging 0 to 1)
(X-axis: Z-Rotation error (degrees) yes degrees!!, ranging 0 to 2.5)

Periscope grouped mirror pairs

The axial Z displacement tolerance is 10's of millimeters (no plot). Not surprising since we would expect a large depth of field.

# Appendix 2: Ball System Study

1.   Introduction

The MAXIM (Mico-Arcsecond X-Ray Imaging Mission) and MAXIM Pathfinder, a technology precursor mission, are considered by NASA as "visionary missions" in space astronomy.   As proposed, the MAXIM mission would fly in formation 32 spacecraft, each carrying precision optics to direct stellar emitted X-rays to a collector and imaging spacecraft. The mission architecture is complex and provides technical challenges in formation flying and external metrology, spacecraft pointing control, active internal spacecraft metrology, and target acquisition.

To further develop the concept, an integrated model (IM) of the MAXIM and MAXIM Pathfinder was developed. The IM has been used on numerous other large scale telescope programs such as VLT, NGST, and TPF.   The individual discipline models in structural dynamics, optics, controls, signal processing, detector physics and disturbance modeling are seamlessly integrated into one cohesive model to efficiently support system level trades and analysis. The core of the model is formed by the optical toolbox implemented in MATLAB and realized in object-oriented Simulink environment.   Both geometric and physical optical models can be constructed and interfaced to disturbances and detection models.

Surrounding the coupled optical/structure model is the outer spacecraft attitude control system and external metrology measurements for formation control. The developing integrated system model has supported the MAXIM system engineering effort from the early studies and will be continued to be refined to provide support through launch and on-orbit operation. This report describes the current integrated model (IM) and issues related to it's development, the discipline models used to build up the IM and the results obtained to date.

Two different designs were investigated – the X-configuration and the periscope or P-configuration. To take advantage of the IM capabilities as a system modeling tool, a CAD design was constructed to investigate structural dynamic interactions with the optics to be evaluated. The two designs are shown in Figures 1 and 2.

Figure 1 – CAD design of MAXIM X-configuration

Figure 2 – P-configuration MAXIM CAD design
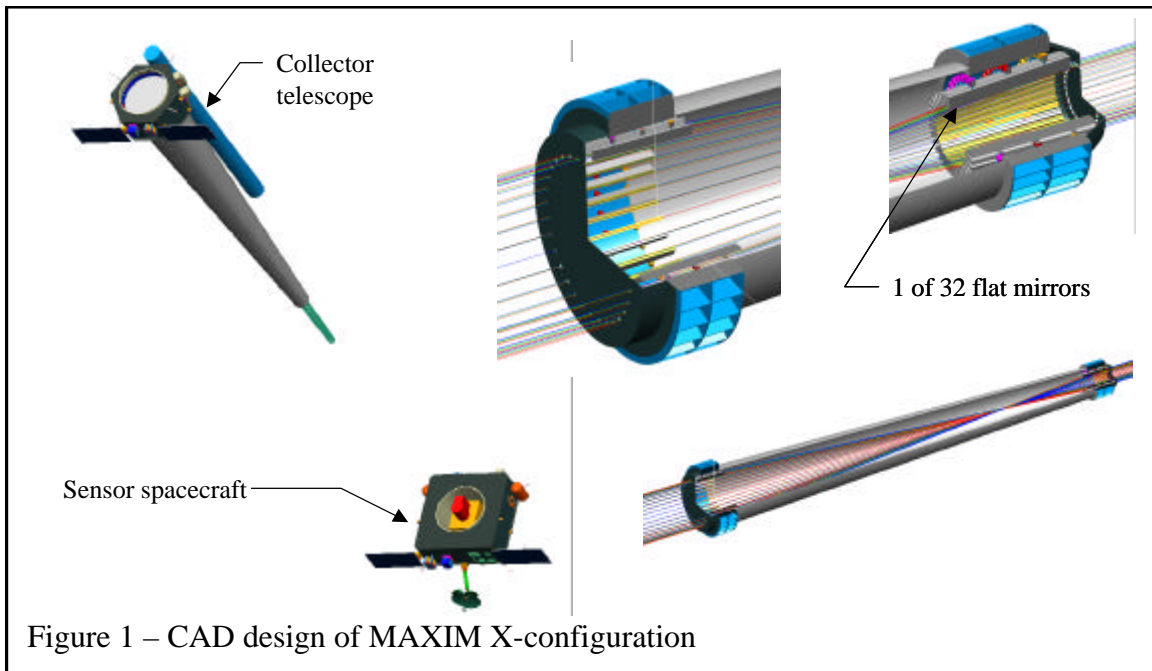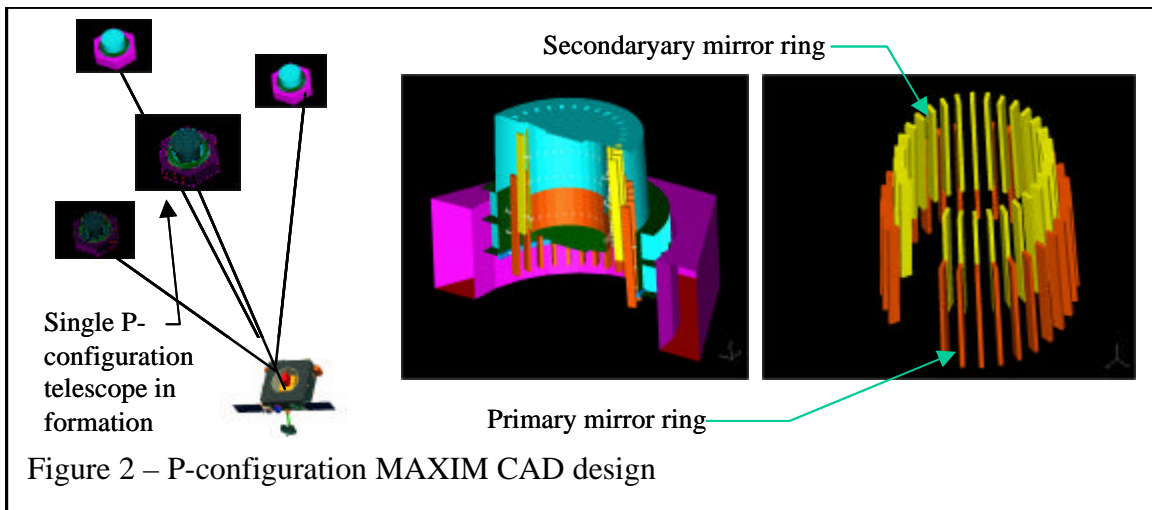
2. Methodology

In this section, the methodology and approach to integrated modeling will be described. The role of integrated modeling in the system engineering process is outlined in Figure 3. The standard process of system development and optimization is shown with a new box inserted to show the role of integrated modeling. The original end-to-end process using only discipline models is shown to provide a methodology for achieving end-to-end results. A parallel path based upon use of integrated model is a very efficient method for optimizing system performance. The discipline models are used for all the detailed design studies, leveraging heavily upon the expertise inherent in the engineers using legacy code such as NASTRAN. Subsystem optimization can also be done at the discipline model level but with guidance provided by interaction with the IM process. There is significant overlap between the work at the two levels - this should be viewed as an advantage for cross-checking results and software validation of the integrated model with the legacy code results.

Figure 3 - System engineering role of integrated modeling
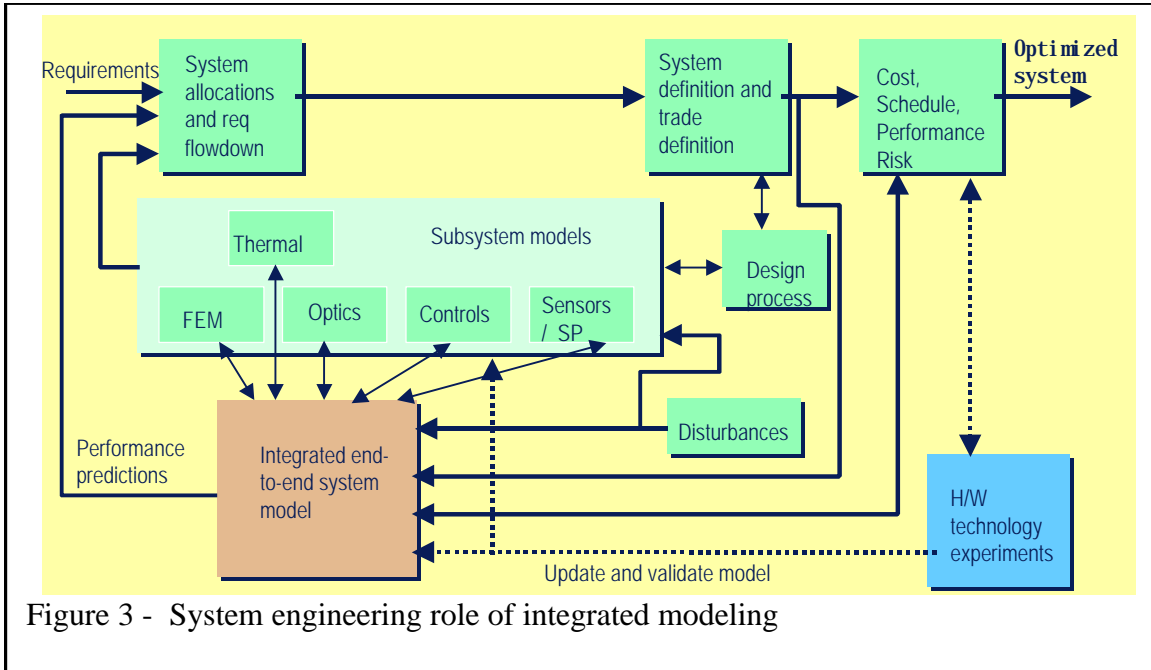
3. Model description and results

In this section the IM models and discipline models are described, and some results obtained with these models are presented. A brief description is given of the IM followed by more detailed description of the discipline model. The overall Simulink model is shown in Figure 4. The key subsystems are represented, with detailed blocks layered below. Simulink allows one to develop detailed layered models and the figure shows only the top levels.

3.1 Optical subsystem

The optics modeling module for the IM consists of an Optical Toolbox written in MATLAB with an overlay of the Simulink environment. The input to the optical model is the location and orientation of the optical elements. Two models were developed – one for the X-configuration of the optics with 32 mirror flats for both primary and secondary rings, and a periscope version also with 32 mirrors. The placement of all the optics and the number of mirrors can be readily changed for sensitivity studies.

The capabilities of the optical model are:
Geometric ray tracing and computation of the optical path difference (OPD)
Diffractive optics computation of the point spread function (PSF)
Both Fresnel and Fraunhofer wavefront propagation routines
Polarization effects (hasn't been required to date)
Wide FOV/ high resolution PSF images using sparse matrix routines
Transmissibility for each optical element (action is on each ray in the bundle)
Coherent and incoherent image generation
Sensitivity matrix generation
Inclusion of thermal distortion of optical elements
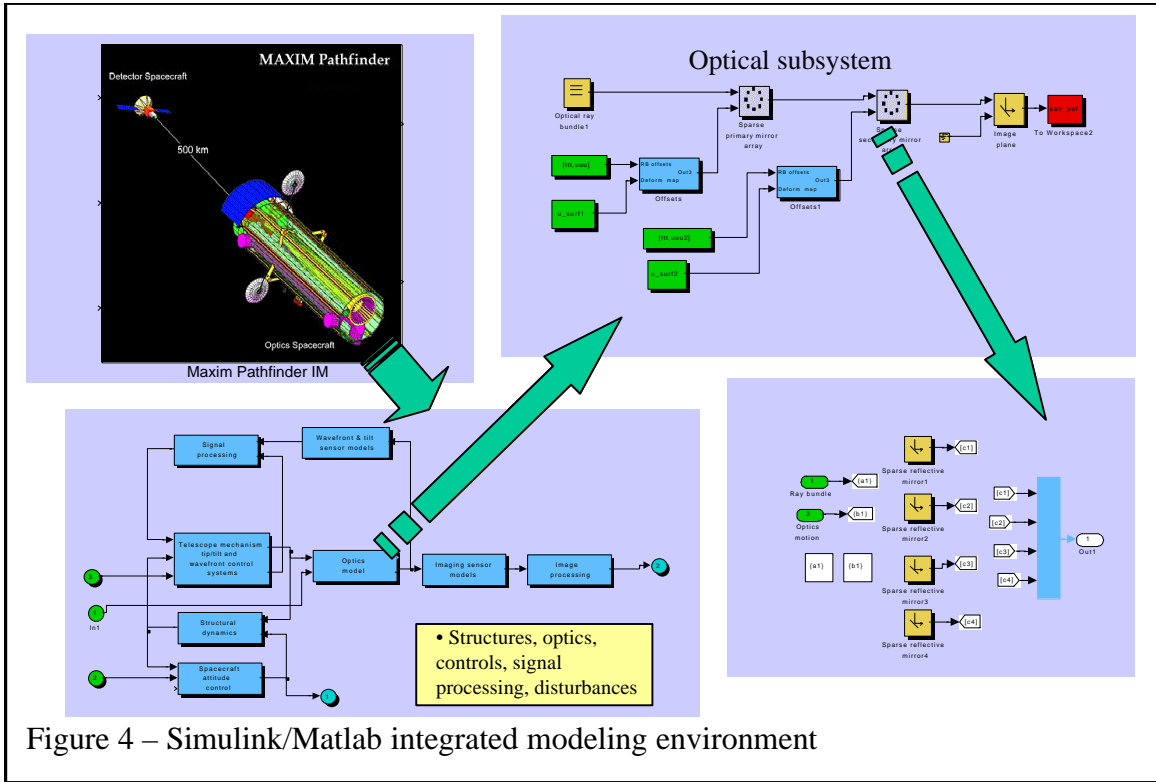Introduction of dynamic motion effects from structural dynamics model outputs

Figure 4 – Simulink/Matlab integrated modeling environment

To run the model, a ray bundle (assuming a point source at infinity) is introduced into each optical surface (32 nominally) and followed to a reference sphere centered on the focal plane – here the optical path difference (OPD) is computed. The OPD mesh is padded with zeros to increase resolution of the PSF. Using the wavefront propagator, the field is computed and the images from each path through the flats added coherently. The PSF is generated by multiplying the field times the conjugate.

3.2 Optical modeling results

The ray trace used a 11x11 grid for each of the 32 optical flats to the focus 456 km distant on a separate spacecraft. The ray trace generated by the optical part of the IM is shown for both the X-configuration and the periscope configuration in Figure 5. The ray trace from the secondary to the focus is shown on a log scale while the rest is at a regular scale. For the X-configuration, the grazing angle is 2.42058 degrees and the nominal wavelength set at 2 nm (0.62kV). The primary /secondary separation was set at 10 m and the ring diameters were respectively 1.4 and 0.3 m. For the periscope or P configuration, the grazing angle was 2 degrees at the same nominal wavelength and the primary/ secondary separation set at 0.45 meters. The diameters were 1.4 and 1.334 m respectively.

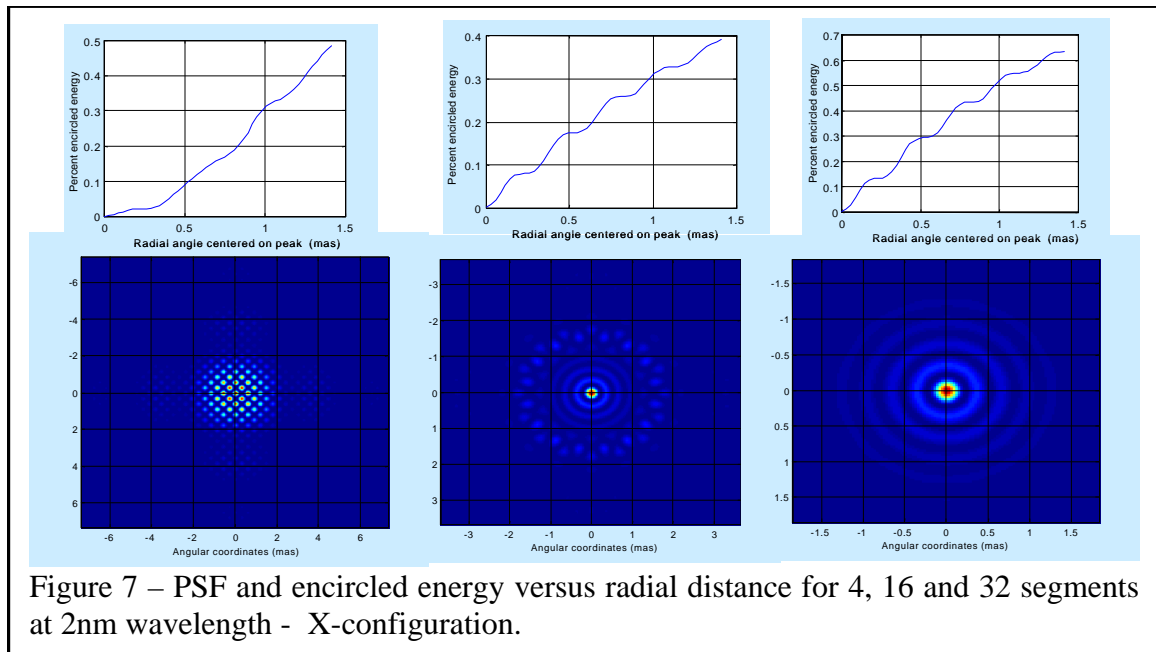Figure 5 – Ray trace of X-configuration and P-configuration
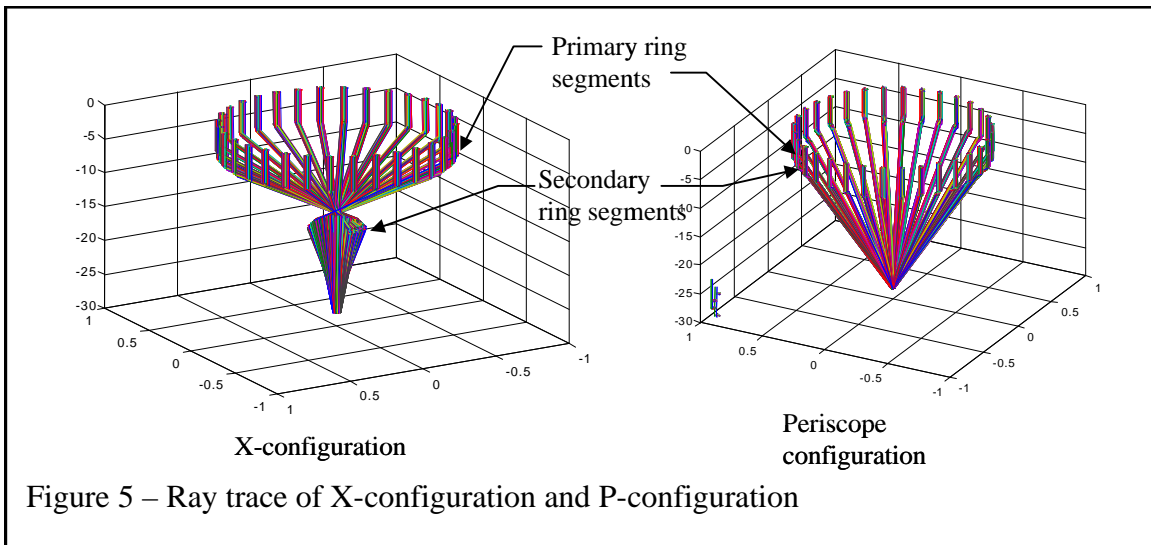
Because the optical surfaces are flats instead of curved surfaces, a spherical wavefront error is created when the wavefront is referenced to a spherical surface. This effect is shown in the OPD plots of the wavefront error for 4 representative surfaces shown in Figure 6. The peak/valley wavefront error is ~0.4 nm or 1/5 a wave at 2 nm. Obviously, increasing the focal length decreases this wavefront error.

Figure 6 – Wavefront error on 4 opposing segments due to use of flat optics
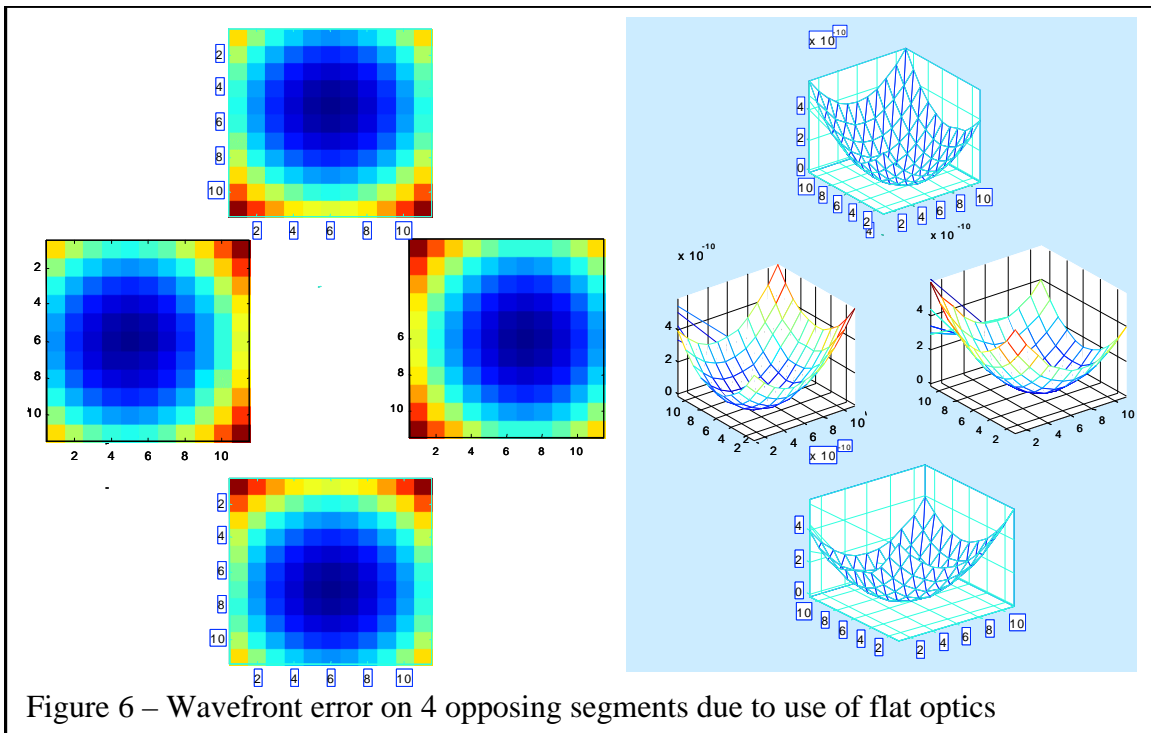
The effect on the resulting point spread functions is in the following images in Figures 7 and 8 for the X-configuration. The a running summing of the enclosed power in the PSF is shown above of an image of the PSF for 4, 16 and 32 segment configuration (left to right). One can see in Figure 5 that the power in the first ring is approximately 14 percent at 2 nm wavelength for the 32 segment case and drops to ~2.5 percent for 4 segments. In figure 6, the wavelength is now 0.62 nm (2 kV), and the energy in the first ring has dropped dramatically due to the spherical error from using a flat optical surface. A lot of the energy is contained in the far out ring structure. This suggest smaller flats may required at shorter wavelengths or perhaps easier, moving the detector spacecraft further out by a factor of ~3 will produce the same image at 0.62nm as at 2nm. Note, axes scaling on both axes)Figures 7 and 8) should be corrected by a factor 2x. For reference purposes, the diameter of the PSF for a optical ring at 2 nm is 2.239e-9 nrad.

The periscope configuration produces the following PSF's at 450 km distance (see Figure 9). Note that the for the 32 segment configuration the encircled energy in the first ring has diminished from 14 to 10 percent.

Figure 7 – PSF and encircled energy versus radial distance for 4, 16 and 32 segments at 2nm wavelength - X-configuration.
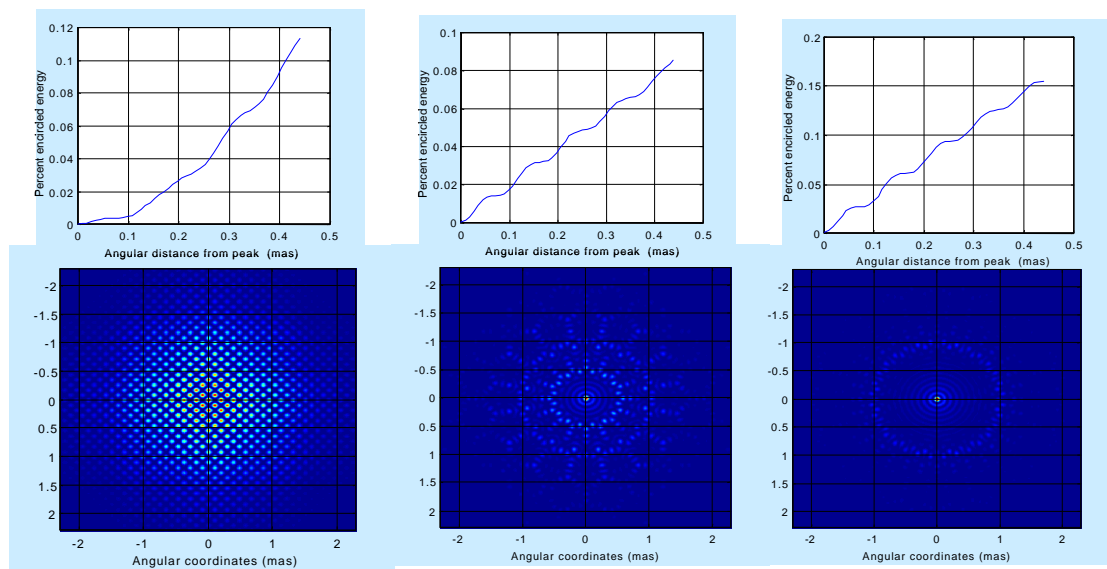
Figure 8 - PSF and encircled energy versus radial distance for 4, 16 and 32 segments at 0.62 nm wavelength – X-configuration.
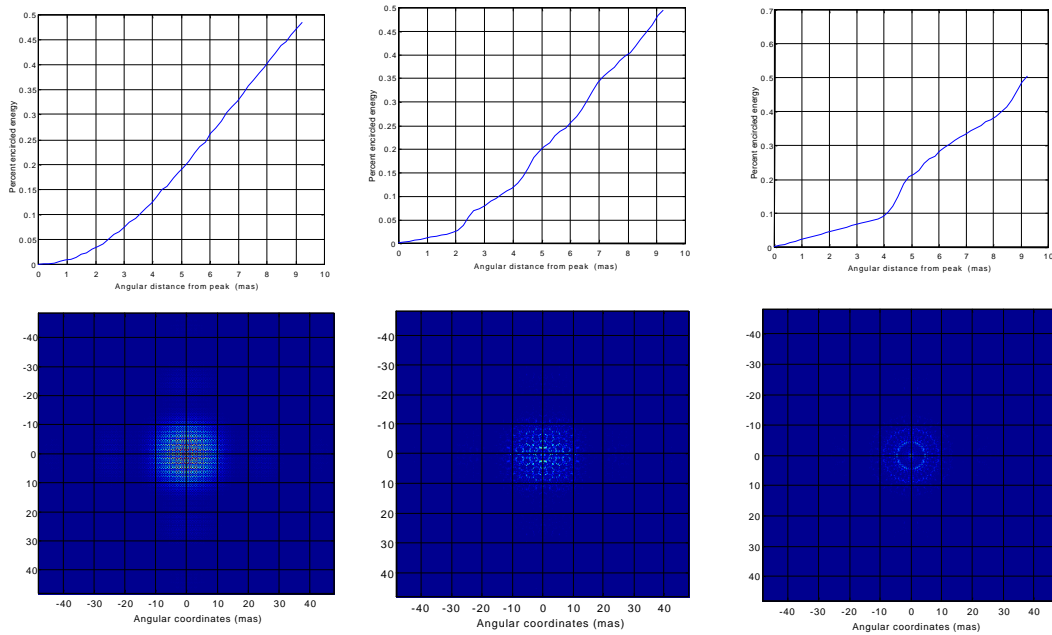

Figure 9 – PSF and encircled energy versus radial distance for 4, 16 and 32 segments at 0.62 nm wavelength – P-configuration.

One surprise with the X-configuration was its sensitivity to off-axis imaging effects. In Figure 10 the point source was moved off-axis 10 nrads and a PSF formed for 4, 16 and 32 segments. The energy in the wings is found to shift from one side to the other as commonly caused by coma. At 30 nrads, this effect is severe enough to limit the field of view. The P-configuration design was studied in more depth other optical modeling tools and found to be much less sensitive to off-axis images.

Figure 10 – Coma introduced into PSF from offaxis image.
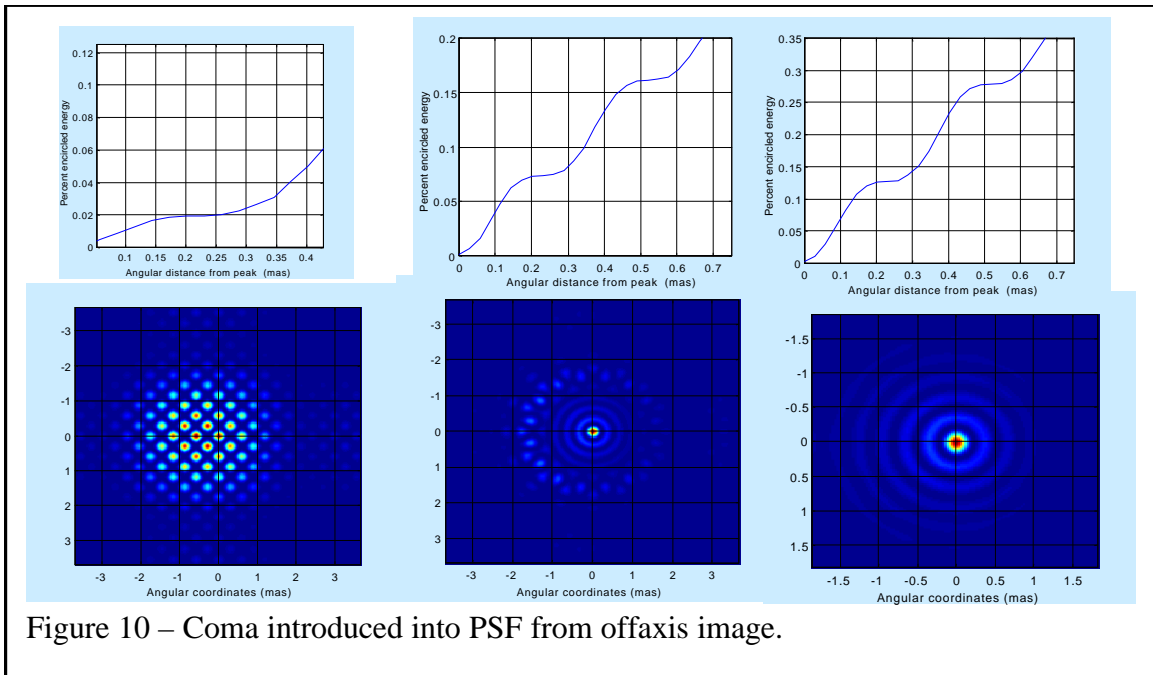
Overall, the P-configuration is a much better design due to wider FOV, significantly more compact design and most importantly, the photon collection is ~4x larger for the P-configuration for the same primary diameter. This is because for both designs the aperture stop is set by the secondary ring of mirrors and the secondary for the P-configuration is almost the same size as the primary mirror ring.

### 3.3   Image motion due to dynamic disturbances

The dynamic model consists first of the combiner spacecraft/telescope with 5 reaction wheels on isolators. The structural dynamics model was created from the NASTRAN FEM model of the CAD design shown previously. A state space structural dynamics model was created from the first 50 modes. The input disturbance was a set of 5 reaction wheels mounted to a pallet fot attitude control of the telescope. These wheels were originally sized for another mission operating in an L2 orbit and considered close enough for approximate analysis. The wheels are assumed mounted to a 6 DOF node on the spacecraft and the ouputs of the structural model were the 32 primary and secondary nodes on each mirror. This gave 64 total outputs with 6 DOF each. The structure was assumed to have 0.5% damping. To evaluate the jitter created at the final image, a set of optical sensitivity matrices were generated by perturbing the optical system in all directions for every optical element. These optical sensitivity matrices are multiplied times the structural output motion to get image motion. Therefore, the forces from all 5 wheels are applied to the structure and the resulting output jitter from there combined effect is root sum squared together to get the jitter. Each wheel model has a fundamental harmonic disturbance and multiples of these harmonics. The generated forces and torques increase with the square of the wheel speed. Therefore, the resulting plot shows the RSS'd jitter as a function of wheel speed.
The wheels are assumed to be balanced to the level in the HST and the data used was from actual data from Honeywell.

The model of the reaction wheel used is shown at 10rps and at 45 rps – note the increasing output forces. The largest structural transfer functions for x and y inputs are shown with the input of force and the output in units of displacement.

Figure 11 shows the process and the final results of jitter on the focal plane. Note that the structural model has its first significant mode at 40 Hz which means this structure is very stiff. With more fidelity, this first mode can be expected to drop to a lower value. The result shows that with no isolation the rigid body motion is approximately 0.08 mas and building to 10 mas at higher speeds. With an isolator with 0.2 percent damping, and stifnesses corrresponding to 4 and 1.5 Hz the jitter drops significantly. Normally one would assume about 1/10 of a pixel (~0.044mas) as a goal for diffraction limited sytems. However, since this is a photon counting system, we can relax this significantly. This area needs further exploration, but the initial recommendation would be to explore microthrusters dues to their much lower disturbances generated.
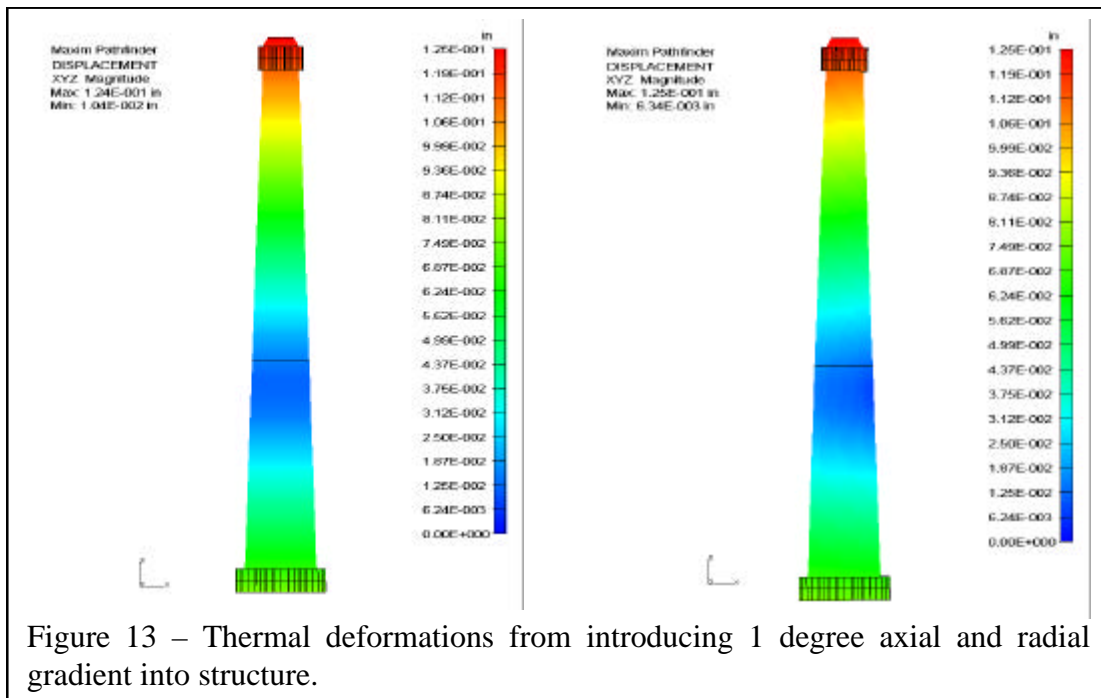

Figure 11 – Reaction wheel harmonics disturbances and resulting focal plane jitter.
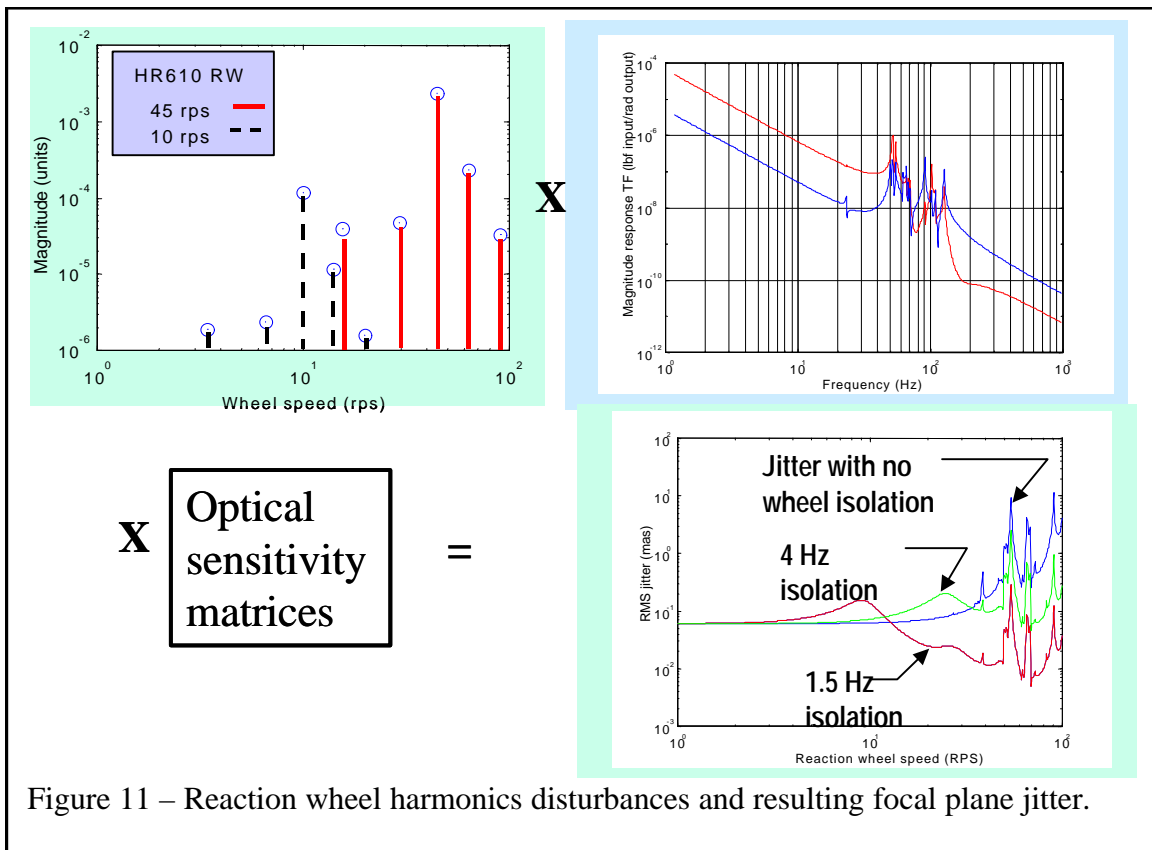
The mode shapes for the first five modes are the tower bending modes. These are included in Figure 12 for reference purposes.

Figure 12 – First five bending modes of the collector telescope
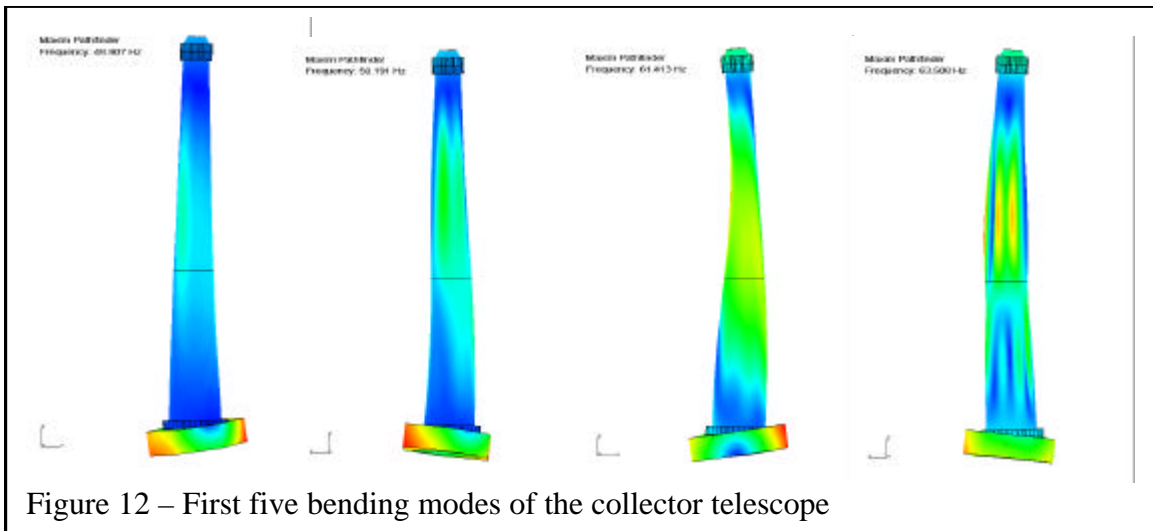
3.4 Thermal modeling

An attempt was made to evaluate thermal sensitivity by applying a 1 degree thermal gradient across the telescope in both a radial and axial direction. The results seemed counterintuitive and the correctness of the model needs to be further evaluated. Therefore the resulting displacement field effects on the optical performance were not computed. The main distortion was an axial growth of the telescope as shown in Figure 13.

Figure 13 – Thermal deformations from introducing 1 degree axial and radial gradient into structure.

4.0   Further modeling and system engineering

This effort along with other design and analysis by NASA , CU and at Ball have helped to better define the requirements for the MAXIM program. Several areas need further attention and these are listed below.

- Internal and external metrology
- Optical element requirement in terms of allowable wavefront error
- Metrolgy sensor type and models for
- Formation flying interaction with individual elements
- Thermal stability
- Microthrusters performance
- System error budgeting
- More detail on technology development paths